

Sl. No.	<p style="text-align: center;">IIT Ropar List of Recent Publications with Abstract Coverage: May, 2025</p>
A	<p style="text-align: center;">Conference Proceeding(s)</p>
1.	<p><u>A comparative experimental investigation on charging and discharging of paraffin wax PCM with surface and volume heating approach</u> AS Kashyap, V Bhalla, H Tyagi - 9th World Congress on Momentum, Heat and Mass Transfer (MHMT), 2024</p> <p>Abstract: Solar energy is a promising alternative to fossil fuels for various domestic and industrial thermal applications. However, to deal with its intermittent nature, solar thermal energy storage (STES) is a promising technology for continuous and sustainable operation.</p> <p>This study presents an experimental investigation for the complete charging-discharging cycle of paraffin wax PCM with surface and volume heating. Surface heating has been abbreviated as SH, and volume heating as VH. The comparison in both studies has been made based on temperature rise at the end of the charging process. The SH shows a temperature rise of 67.28 °C, while with the VH, a temperature rise of 59.25 °C is obtained. The effect of variation in heat flux has also been investigated by varying the distance between the light source (halogen lamp) and the receiver (glass beaker filled with paraffin wax). A decrease of 16.01 °C is obtained for the SH when the distance has been increased from 8 to 10 cm. From the results, it is concluded that SH is a more promising approach than VH without the optical properties enhancement of paraffin wax.</p>
2.	<p><u>A parasitic strip loaded broadband circularly polarized antenna for 5 GHz WBAN full-duplexing</u> A Thakur, A Sharma - National Conference on Communications (NCC), 2025</p> <p>Abstract: Wearable antennas operating in the 5 GHz (5.15 – 5.825 GHz) have gained increasing attention due to their promising potential, offering approximately 1 GHz of bandwidth and data rates up to 10 Gb/s. This study introduces a parasitic strip-loaded, low profile, dual circularly polarized (DCP) antenna for 5 GHz WBAN (wireless body area network) applications. A semi-flexible Rogger 5880 substrate is used to design the proposed structure. Performance improvements in impedance bandwidth (IBW), port isolation and axial ratio (AR) bandwidth are achieved through the integration of two parasitic strips positioned or-thogonally to the feed lines. The antenna demonstrates co/cross-polarization isolation of over 18 dB, making it highly suitable for full-duplex WBAN applications. For robustness evaluation, simulations on a human body model are conducted, revealing a maximum specific absorption rate (SAR) of 1.22 w/kg, ensuring compliance with safety standards. The measured peak gain of 3.4 dBi is observed in the free space with port isolation > 26 dB in the band of interest (5.15 – 5.825 GHz). These attributes make the proposed antenna an optimal solution for 5 GHz WBAN full-duplexing.</p>
3.	<p><u>Advancements in mechanical biosensors for the detection and measurement of biological molecules: A review</u> B Borthakur, P Borthakur - 5th International Electronic Conference on Biosensors, 2025</p> <p>Abstract: Mechanical biosensors represent a cutting-edge analytical technology for detecting and measuring biological molecules with unparalleled precision and sensitivity. These innovative devices rely on the integration of biological recognition elements and mechanical transducers to convert molecular interactions into quantifiable signals. Their utility spans a range of applications, including healthcare, environmental monitoring, and food safety, making them indispensable in modern analytical sciences. At the heart of mechanical biosensors are bio-receptors, biological components such as enzymes, antibodies, or nucleic acids, which bind selectively to target</p>

	<p>molecules. These bioreceptors are immobilized on transducer surfaces using techniques like physical adsorption, covalent bonding, or entrapment, ensuring stable and specific interactions even in complex biological matrices. Advancements in sensor design and material sciences have significantly enhanced the performance of mechanical biosensors. Embedding magnetic elements such as Fe₃O₄ nanoparticles amplifies detection sensitivity. Mechanical biosensors detect target molecules through surface stress measurement, mass detection, and force sensing. These capabilities make them highly versatile, with applications in medical diagnostics for detecting disease biomarkers, environmental monitoring for identifying pollutants, and food safety for detecting contaminants such as pathogens and chemical residues. Despite their advancements, challenges remain, including minimizing non-specific interactions and improving sensor reproducibility. Future innovations are expected to integrate nanotechnology, multi-analyte detection capabilities, and compact designs for wearable and portable applications.</p>
4.	<p>Analytical study on Class II Bragg resonance of surface wave interaction under the effect of current and surface tension D Goyal, TK Hota, SC Martha - 40th International Workshop on Water Waves and Floating Bodies, 2025</p> <p>Highlights: Class II Bragg resonance is investigated in a channel when the surface waves interact with bottom morphology of composite sinusoidal bars in the presence of current and surface tension. A multi-scale expansion technique is used to obtain the expressions for reflection and transmission coefficients analytically with the advantage of uniformly valid solutions. Current plays a very significant role in altering the Bragg resonance properties including the phase shift, amplitude and asymmetrical patterns in subharmonic peaks for reflection. Depending upon current strength, number of ripples varies to attain almost 100% reflection. The study is highly beneficial in the coastal areas where Bragg resonance occurs in the presence of ocean currents.</p>
5.	<p>Comparative analysis of AES, RC and twofish algorithms for data encryption and decryption AFB Tajuddin, MHM Yusof, M Balfaqih, AA Almohammed, S Darshi, N Qaid - 4th International Conference on Computing and Information Technology (ICCIT), 2025</p> <p>Abstract: This paper presents a comparative analysis of three widely used encryption algorithms, namely AES (Advanced Encryption Standard), RC (Rivest Cipher), and Twofish, with a focus on their performance in data encryption and decryption. The study aims to evaluate the strengths and weaknesses of these algorithms in terms of security, speed, and efficiency. The analysis involves benchmarking the algorithms against various performance metrics, including encryption time, decryption time, key size, and resistance against cryptanalysis attacks. Additionally, the research explores the impact of different data sizes and configurations on the performance of each algorithm. The findings of this study will provide valuable insights for decision-makers and practitioners in selecting the most suitable encryption algorithm for their specific needs, considering the tradeoffs between security and performance.</p>
6.	<p>Creeping flow of shear-thinning fluids through an orifice N Dutt, SA Patel - Conference on Fluid Mechanics and Fluid Power, 2025</p>

	<p>Abstract: In this study, the two-dimensional creeping flow of shear-thinning fluids through a square-edged concentric orifice in a pipe has been analysed numerically over a wide range of orifice plate thickness, $1/16 \leq \gamma \leq 1$ with fixed diameter ratio of the orifice to pipe, $\beta = 0.5$. The numerical result has been derived over the range of power-law index, $0.2 \leq n \leq 1$ to analyse the discharge coefficient as an important parameter while using an orifice meter as a flow measuring device for shear-thinning fluids. The influence of the orifice plate thickness (γ) and power-law index (n) on the discharge coefficient has been studied in detail. Further flow field has been examined in terms of velocity contours, viscosity contours, and streamline patterns over the range of thickness of the orifice and power-law index. A comparison has been made between two different types of pressure tapings, i.e., D–D/2 taps and corner taps for the entire thickness-to-diameter ratio taken into consideration. In addition, a correlation has been established for the discharge coefficient as relation to orifice thickness and power-law index thereby enabling their interpolation for the intermediate values in various applications.</p>
7.	<p><u>Energy-efficient MQTT protocol based processing architecture for water monitoring application</u> K Singh, S Kumar - National Conference on Communications (NCC), 2025</p> <p>Abstract: Water quality monitoring (WQM) is indispensable as several industries discharge hazardous chemicals and waste directly into the rivers, contaminating the water resources. Numerous existing systems provide WQM but are not energy-efficient solutions as they transmit huge amounts of data on cloud servers at regular intervals. Additionally, incorporating Deep Neural Network (DNN) models on the cloud for data inferencing results in high-cost consumption. Thus, this study provides a dynamic payload-based energy-efficient solution that integrates a lightweight Message Queuing Telemetry Transport (MQTT) protocol for wireless communication between the WQM sensor node and the cloud server. The proposed system is built on a resource-constrained ATMEGA2560-16AU microcontroller platform that provides real-time data and makes a cost-effective solution. Quectel EC200U-CN module provides a 4G connection for data transmission and consumes maximum current during transmission. Hence, the presented architecture establishes a reliable connection and transmits dynamic payload constructing water quality (WQ) parameters to the cloud server whenever a significant change is noticed via the proposed set of sequences of AT commands. The lower root mean squared error (RSME) and higher R-squared value comparison between the sensor node data at the edge and stored data at the cloud server remarks the efficiency of the proposed architecture with reduced energy consumption. Moreover, the system sends alert notifications on the developed web application for quick remedial actions at alarming conditions.</p>
8.	<p><u>Frequency-dependent mutual inductance in broadside-coupled superconducting striplines</u> VK Nishad, AK Nishad - IEEE 29th Workshop on Signal and Power Integrity (SPI), 2025</p> <p>Abstract: This study examines the mutual inductance that depends on the frequency of broadside-coupled superconducting striplines fabricated via the SFQ5ee process. Using Zimmermann's complex conductivity model put into a frequency-related surface impedance setup, mutual inductance was determined for striplines of widths $w=0.25\mu\text{ m}, 0.35\mu\text{ m}$, and $0.5\mu\text{ m}$ through HFSS simulations. The findings show that mutual inductance increases as the width of the stripline decreases and becomes steady at lower frequencies. At the gap frequency, the HFSS simulations were very precise, with a maximum error of only 1.1 % when compared to the experimental data, which is much better than the wxLC simulations with errors as high as 9 %. These results improve our knowledge of the mutual inductance in submicron superconducting striplines and offer a reliable method for designing and enhancing scalable superconducting integrated circuits.</p>
9.	<p><u>GAMSRN: Global attention multi-scale residual network for single-image super-resolution and low-light enhancement</u> Inderjeet, JS Sahambi - National Conference on Communications (NCC), 2025</p>

	<p>Abstract: The deep convolutional neural network (CNN) has achieved significant success in image restoration (IR). However, most deep neural networks use a single-sized convolution kernel to capture spatial information, limiting local feature extraction. Additionally, since convolution is designed for local operations, it struggles to capture the inherent global characteristics of an image. This paper addresses these issues by proposing a novel global attention multi-scale residual network (GAMSRN) based on global attention and multi-scale feature extraction. The network employs global attention multi-scale residual blocks (GAMSRB) that use convolution kernels with uniform sizes but varying dilation rates to extract features at different scales without increasing model complexity. Furthermore, the attention mechanism effectively models global features and enhances the network's expressiveness. These components together enhance performance. Our proposed network is generalizable for two applications: super-resolution and low-light enhancement. Extensive qualitative and quantitative comparison with six synthetic benchmark datasets demonstrates the efficacy of our proposed GAMSRN over reported works.</p>
10.	<p>High frequency analysis of Cu-CNT based tapered TSV bumps MG Kumar, Y Agrawal, R Sharma - IEEE 29th Workshop on Signal and Power Integrity (SPI), 2025</p> <p>Abstract: In latest development of three-dimensional integrated circuit technology, tapered through silicon via (TSV) bumps are becoming a popular alternative to traditional cylindrical structure due to extremely low coupling and volume fraction, which leads to reduced crosstalk delay and better signal integrity. The tapered TSV bump structure is filled with Cu-CNT composite, which can exhibit better mechanical, thermal and electrical properties. The electrical equivalent for tapered TSV has been modeled along with redistribution layer (RDL). In this work, crosstalk and power loss analyses have been carried out. Further, we report that Cu-CNT composite TSVs outperform Cu and CNT TSVs. In addition, analysis of the different bump structures has been presented in this paper.</p>
11.	<p>(Independent) Roman domination parameterized by distance to cluster P Ashok, GK Das, A Pandey, K Paul, S Paul - International Conference on Combinatorial Optimization and Applications (COCOAA), 2025</p> <p>Abstract: Given a graph $G=(V,E)$, a function $f:V \rightarrow \{0,1,2\}$ is said to be a Roman Dominating function (RDF) if for every $v \in V$ with $f(v)=0$, there exists a vertex $u \in N(v)$ such that $f(u)=2$. A Roman Dominating function f is said to be an Independent Roman Dominating function (IRDF), if $V_1 \cup V_2$ forms an independent set, where $V_i = \{v \in V \mid f(v)=i\}$, for $i \in \{0,1,2\}$. The total weight of f is equal to $\sum_{v \in V} f(v)$, and is denoted as $w(f)$. The Roman Domination Number (resp. Independent Roman Domination Number) of G, denoted by $\gamma_R(G)$ (resp. $i_R(G)$), is defined as $\min\{w(f) \mid f \text{ is an RDF (resp. IRDF) of } G\}$. For a given graph G, the problem of computing $\gamma_R(G)$ (resp. $i_R(G)$) is defined as the Roman Domination problem (resp. Independent Roman Domination problem).</p> <p>In this paper, we examine structural parameterizations of the (Independent) Roman Domination problem. We propose fixed-parameter tractable (FPT) algorithms for the (Independent) Roman Domination problem in graphs that are k vertices away from a cluster graph. These graphs have a set of k vertices whose removal results in a cluster graph. We refer to k as the distance to the cluster graph. Specifically, we prove the following results when parameterized by the deletion distance k to cluster graphs: we can find the Roman Domination Number (and Independent Roman Domination Number) in time $4^k n^{O(1)}$. In terms of lower bounds, we show that the Roman Domination number can not be computed in time $2^{\epsilon k} n^{O(1)}$, for any $0 < \epsilon < 1$ unless a well-known conjecture, SETH fails. In addition, we also show that the Roman Domination problem, parameterized by distance to cluster, does not admit a polynomial kernel unless $NP \subseteq coNP/poly$.</p>

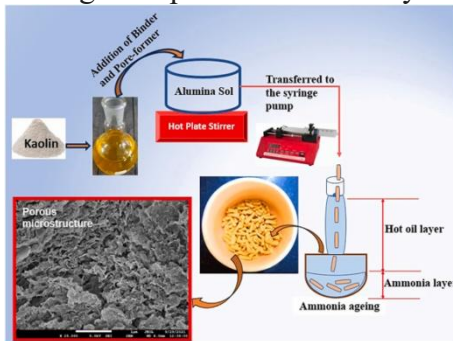
12.	<p><u>Impact of scaling on large crossbar arrays for neuromorphic applications</u> S Kushwaha, CB Rao, Shamini P. R, S Roy, R Sharma - IEEE 29th Workshop on Signal and Power Integrity (SPI), 2025</p> <p>Abstract: Large-scale crossbar arrays form the functional building block for neural networks that perform efficient inmemory computing with massive parallelism. In this paper, the impact of scaling of nano interconnects in large-sized crossbar arrays for neuromorphic applications is presented. Nanoscale interconnects are used to generate significantly larger crossbar arrays like 64×64, 128×128 and 256×256 considering 13 nm and 7 nm technology nodes. These crossbar arrays are analyzed to study the effects of technology scaling and large arrays sizing on the key performance metrics like delay time, rise time and fall time.</p>
13.	<p><u>Laminar combined convection in pseudoplastic fluids from a horizontal cylinder in an adiabatic channel</u> K Aherwar, N Dutt, P Suri, SA Patel - Conference on Fluid Mechanics and Fluid Power(FMFP), 2025</p> <p>Abstract: The laminar combined free and forced convection is studied in pseudoplastic or shear-thinning fluids flowing past a confined horizontal cylinder. The forced flow is directed normal to the direction of thermal buoyancy in a confined channel with adiabatic walls. The study expands the results over the range of pseudoplastic fluids varying in the power-law index, n from 0.3 to 1, including Newtonian fluid as a limiting case. The effect of non-dimensional parameters on the cross-buoyancy flow, Prandtl number, $1 \leq Pr \leq 100$, Reynolds number, $1 \leq Re \leq 20$, Richardson number, $0 \leq Ri \leq 3$, and Grashof number, $10 \leq Gr \leq 10^5$ have been explored for two values of cylinder confinement B, defined as the diameter of cylinder to height of the channel, $D/H = 1/10$, $1/5$. The governing equations have been solved for the steady-state flow over the range of parameters by employing finite-element numerical scheme. The flow and thermal field distorted by cross-buoyancy past a hot cylinder is analysed by plotting the streamlines and isotherms in the channel. The total drag, lift coefficients, and average Nusselt number increase as the confinement ratio, B increases from $1/10$ to $1/5$. At $Ri = 3$ for $B = 1/5$, the flow reversal adjacent to the wall in the downstream section of the cylinder has been observed at $Re = 20$ for $Pr = 1$ which is abolished as the shear-thinning effect of fluid decreases. Finally, a correlation to predict the average Nusselt number as $Nu_{avg} = f(Re, Pr, Ri, n)$ for both the confinements has been proposed over the range of parameters.</p>
14.	<p><u>Micropile as slope remediation in dynamic slope stability analysis of a slope failure in Kullu: Case study</u> S Kushwaha, RM Kannan, U Veena, N James - International Conference on Recent Advances in Geotechnical Earthquake Engineering and Soil Dynamics, 2025</p> <p>Abstract: The severity and frequency of landslides are increasing each year, posing a growing concern. Around the world, landslides are becoming more prevalent, with India being one of the most affected countries. According to the Geological Survey of India (GSI), 12.6% of India's land area is in a hazardous zone that is prone to landslides, resulting in significant loss of life and economy. Himachal Pradesh, a state in northern India characterized by its steep terrain which constitutes 25% of total landslide vulnerable area, often experiences such tragedies yearly due to the tectonic movements, rising trend of monsoonal rainfall and growing population in the region. This region experiences less seismic-induced landslides than rainfall-induced ones, but the long-term effects of both may worsen the situation. Thus, this study is an attempt to analyze slope stability by examining the combined effects of seismic activity and rainfall over a time interval to understand its long-term stability performance. For this, a susceptible area from Kullu region is selected to assess the stability analysis in its prevailing condition. Field surveys, field testing and laboratory tests are conducted to characterize the soil properties and slope profiles. Further, a</p>

	comparative analysis of the slope with and without the remediation measure is performed to assess the performance of the remediation. Due to the geotechnical characteristics examined for the site and considering Federal Highway Administration (FHWA) recommendations, providing a micropile is considered a suitable remedial measure. The assessment highlights the micropile installation as an effective remedial measure to safeguard the slope, the adjacent National Highway and the uphill Deodhar village.
15.	<p>Multi-state resistance tuning via voltage ramp rates in Ni/Mo/MoO₃/Ni memristors for high-density memory applications M Praveen, AK Nishad, VK Nishad - IEEE International Conference on Interdisciplinary Approaches in Technology and Management for Social Innovation (IATMSI), 2025</p> <p>Abstract: Multilevel cell (MLC) storage technology holds significant promise for achieving ultra-high-density memory at a reduced cost. In this study, we demonstrate 2-bit-per-cell storage characteristics in a Ni/Mo/MoO₃/Ni memristor device by tuning input voltage ramp rates (VRR) to obtain different compliance currents (ICC). The Simulation results indicate that the ICC of the device is inversely proportional to VRR, while VSET increases correspondingly. The Ni/Mo/MoO₃/Ni memristor device was designed using the electro-thermal module in the COMSOL Multiphysics tool. The investigation focuses on key MLC operational requirements, particularly switching uniformity and resistance level stability. An engineered stack structure based on thermodynamic principles was developed, comprising a top electrode (Ni), an oxygen vacancy reservoir layer (Mo), a switching layer (MoO₃), and a bottom electrode (Ni). By incorporating a 10-nm Mo layer at the Ni/MoO_x interface, the optimized device exhibited three distinct low-resistance states while maintaining a single high-resistance state. These states were achieved under different voltage ramp rates— 100 V/s, 10 kV/s, and 1 MV/s—resulting in varying compliance currents (ICC) and VSET values. It is attributed to filament confinement that the switching performance and MLC behavior are improved. According to electrical measurements, this confinement produces favorable electric fields that promote the formation of thin and highly conductive filaments. These findings underscore the potential of the Ni/Mo/MoO₃/Ni memristor for advanced MLC memory applications.</p>
16.	<p>Next-gen farming: Real-time monitoring of soil phosphate levels using P sensor G Kumar, L Kumar, D Garg, N Halder, H Singh, YS Diamand - Fourth International Conference on Computing and Communication Networks (ICCCN), 2025</p> <p>Abstract: Precision agriculture is crucial for securing food supplies for the world's expanding population. This research focuses on the critical role of nutrient assessment in data-driven agriculture, specifically targeting phosphorus (P) concentrations. Traditional soil testing methods are often expensive and time-consuming, posing challenges for continuous cropping systems. To address this, a novel chip-level colorimeter for real-time, portable detection of soil P levels is developed. The device operates by inducing a chemical reaction with the soil solution, generating a color change in the presence of nutrients. This color change is quantitatively measured using sensors integrated into a handheld colorimeter or spectrophotometer. Test samples of various standard phosphate solutions were analyzed and validated against laboratory spectrophotometric results. The developed device demonstrates significant potential for environmental and biological applications, offering a cost-effective and efficient solution for maintaining soil fertility and enhancing crop yields. This innovation represents a crucial advancement in smart agriculture, paving the way for sustainable agricultural practices.</p>
17.	<p>Optimization study of power-law fluids staggered circular cylinders in laminar forced convection KK Agarwal, N Dutt, P Suri, SA Patel - 9th World Congress on Momentum, Heat and Mass Transfer (MHMT), 2024</p>

	<p>Abstract: In this study, for power-law fluids, a two-dimensional heat transfer analysis was performed in a circular cylinder to determine the ideal distance between cylinders in equilateral triangle configurations for forced convection in free stream cross-flow. The cylinder array is in contact with a free stream of a specific temperature and velocity while occupying a set volume. The optimal cylinder-to-cylinder spacing is determined by maximizing the overall thermal conductance between all the cylinders and the free stream. The numerical study was conducted to maximize the heat transfer rate over the range of Reynolds number, $40 \leq Re \leq 200$; power-law index, $0.2 \leq n \leq 1.3$; Prandtl number, $1 \leq Pr \leq 100$; and geometries with spacing from cylinder-to-cylinder, $0.5 \leq S/D \leq 2$. The governing equations have been solved for the steady state flow over the range of parameters by employing finite-element numerical scheme. The flow and thermal field by using hot cylinder arranged in triangular array is analysed by plotting the streamlines and isotherms. The thermal heat conductance increases for the shear thinning fluids as Reynolds number increases and on further increasing the Prandtl number. The relation for thermal heat conductance with Prandtl number for extreme values of Reynolds number is also shown for different values of power-law index.</p>
18.	<p>Periodic spatio-temporal colored hotspot detection in azure traffic data R Rajeev, R Jain, VMV Gunturi, V Datta, K Ramesh, A Anshuman, M Gupta, S Jain - Asian Conference on Intelligent Information and Database Systems (ACIIDS), 2025</p> <p>Abstract: The problem of periodic spatio-temporal colored hotspot <i>detection</i> (PST-Col-Hotspot) takes the following input: (a) a spatio-temporal-color event framework E; (b) a collection of events A (over E), where each event is associated with a set of geo-spatial coordinates, a timestamp and a color. Colors are organized into a hierarchy, CH, with white being the root. Given the input, the goal of PST-Col-Hotspot problem is to determine spatial regions which show high “intensity” of events (of a particular color) at certain periodic intervals. The output of the PST-Col-Hotspot detection problem consists of the following: (a) a collection of spatial regions (which show high intensity of events), (b) their respective time intervals of high activity, periodicity values (e.g., daily, weekday-only, etc.), and color according to the given color hierarchy CH. PST-Col-Hotspot detection poses significant challenge for designing a suitable interest measure. The aim over here is to design a mathematical representation of a PST-Col-Hotspot such that it can differentiate interesting periodic patterns from trivial persistent patterns in the dataset. The current state of the art in the area of spatial and spatio-temporal hotspot detection focus on non-colored and non-periodic patterns. In contrast, our proposed approach is able to determine colored periodic hotspots. We experimentally evaluated our proposed algorithm using both real Azure traffic dataset (from Indian region) and synthetic dataset.</p>
19.	<p>Signal integrity analysis of ultra-scaled copper-graphene heterogeneous interconnect structure S Kushwaha, D Das, S Roy, R Sharma - 2024 IEEE Electrical Design of Advanced Packaging and Systems (EDAPS), 2025</p> <p>Abstract: In this paper, a novel copper graphene heterogeneous interconnect structure is proposed that retains the ease of fabrication while offering significantly improved performance. Signal integrity analysis is performed considering insertion loss and eye diagram. The electrical performance of the proposed hetero interconnects is found to be better than the conventional copper interconnects, making these nano-interconnects suitable for back end of line (BEOL) applications.</p>
20.	<p>Spacer optimization using a Neuro-Pso approach for improving FinFET repeater performance in on-chip global MLG NR interconnects AK Jakhar, A Dasgupta, R Sharma, S Roy - 2024 IEEE Electrical Design of Advanced Packaging and Systems (EDAPS), 2025</p>

	<p>Abstract: Spacers are often used in fin-shaped field effect transistors (FinFETs) to increase the ON current at the cost of higher parasitic capacitances. In this paper, a neural network assisted particle swarm optimization technique called neuro-PSO is developed to optimize the geometrical and material parameters of spacers in order to enhance the performance of FinFET based repeaters in on-chip global MLGMR interconnects. The proposed neuro-PSO approach is able to achieve a much smaller power delay product of MLGMR interconnects while requiring a smaller repeater area than what is possible when no spacers are used.</p>
21.	<p>Sustainable stabilization of expansive soil using mango kernel ash and fly ash: A waste management approach K Bhavitha, J Gunde, K Mallikarjuna Rao - Indian Geotechnical Conference, 2025</p> <p>Abstract: Expansive soils present significant challenges due to montmorillonite, which causes swelling and shrinkage upon contact with water. These soils requires stabilization due to their high plasticity, low shear strength, and high compressibility. Various stabilizers are employed to enhance the soil characteristics. This study investigates the use of fly ash (FA) and mango kernel ash (MKA) as stabilizers. Initially, the basic properties of the soil are determined. Subsequently, MKA is added to the soil in percentages of 10, 20, 30 and 50. Atterberg limits and unconfined compressive strength (UCS) tests are conducted on soil samples mixed with MKA. The soil combined with 20% MKA exhibits the maximum UCS after 14 days of curing, thrice that of pure soil. FA is mixed with MKA in different ratios. MKA is added to the soil at a constant percentage of 10%, while FA is added in percentages of 0, 10, 20, and 30% by soil weight. Similarly, MKA is kept constant at 20 and 30%, while FA is added in the same percentage range. This results in fourteen different combinations. Among these, the soil mixed with 20% MKA and 20% FA demonstrates an increase in UCS compared to pure soil, four times greater than untreated soil. This treatment induces the formation of calcite and calcium silicate gel, which XRD and SEM validated. This study demonstrates the effectiveness of using waste ashes to enhance the strength of expansive soil.</p>
B	Journal Article(s)
22.	<p>A note on cyclic MDS and non-MDS matrices T Chatterjee, A Laha - Cryptography and Communications, 2025</p> <p>Abstract: In 1998, Daemen et al. introduced a circulant Maximum Distance Separable (MDS) matrix in the diffusion layer of the Rijndael block cipher, drawing significant attention to circulant MDS matrices. This block cipher is now universally acclaimed as the AES block cipher. In 2016, Liu and Sim introduced cyclic matrices by modifying the permutation of circulant matrices and established the existence of MDS property for orthogonal left-circulant matrices, a notable subclass within cyclic matrices. While circulant matrices have been well-studied in the literature, the properties of cyclic matrices are not. Back in 1961, Friedman introduced g-circulant matrices which form a subclass of cyclic matrices. In this article, we first establish a permutation equivalence between a cyclic matrix and a circulant matrix. We explore properties of cyclic matrices similar to g-circulant matrices. Additionally, we determine the determinant of g-circulant matrices of order $2^d \times 2^d$ and prove that they cannot be simultaneously orthogonal and MDS over a finite field of characteristic 2. Furthermore, we prove that this result holds for any cyclic matrix.</p>
23.	<p>A novel method of preparing high surface area porous gamma alumina granules from kaolin AK Yadav, B Kumar, RM Prasad, S Bhattacharyya - Microporous and Mesoporous Materials, 2025</p> <p>Abstract: Tubular-shaped porous gamma alumina ($\gamma\text{-Al}_2\text{O}_3$) granules were synthesized from an unconventional source of kaolin powder using acid extraction followed by a modified oil-drop</p>

method. Different organic ingredients, including starch, sucrose, and spent tea leaf waste (STLW) and synthetic constituents like PVP and PEG, were utilized as pore-forming additives to make the granules porous and useful for adsorbent application. The resulting γ -Al₂O₃ granules measured approximately 6 mm long and 2 mm in diameter. The influence of various parameters on the granules' formation, morphology, and stability was systematically investigated. The γ -alumina phase formation was confirmed by powder X-ray diffraction (XRD) study and Fourier-transform infrared spectroscopic analysis (FTIR). Surface morphology and specific surface area of the granules were studied using field emission scanning electron microscopy (FESEM) and N₂ adsorption-desorption analysis. The porous structure of the granules was validated through Barrett-Joyner-Halenda (BJH) pore size distribution analysis and FESEM imaging. The γ -alumina granules with starch as a pore-forming additive demonstrated the highest specific surface area. The unimodal distribution of pores in the mesoporous range is standard for all the batches prepared using different pore former, indicating their potential suitability for adsorption applications.



[Anticipating critical transitions in a stochastic macrophage polarization model](#)
SN Chattopadhyay, AK Gupta - Physical Review E, 2025

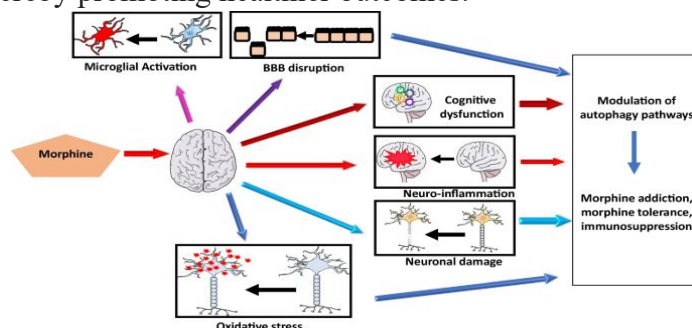
24.

Abstract: As dynamic and adaptable immune system sentinels, macrophages can adopt various functional phenotypes in response to environmental stimuli. The transitions between these states, pro-inflammatory ($M1$), anti-inflammatory ($M2$), and mixed $M1/M2$, are crucial for immune regulation and the pathogenesis of many diseases. Therefore, understanding the parameter domains that enable the coexistence of these phenotypes and the critical values that indicate shifts in macrophage phenotypes is vital. By examining two-parameter phase diagrams and one-parameter bifurcation diagrams, distinct regions of monostability and multistability are identified as cytokine signaling levels (IFN γ and IL-4) change, revealing tipping points for phenotype transitions. All three phenotypes can coexist when the cytokine signals are balanced. The study explores the resilience of macrophage phenotypes through basin stability measures and stochastic potential, highlighting the preservation of a phenotype amid environmental perturbations. Furthermore, it illustrates phenotype shifts using critical transition theory and the predictive power of early warning signals (EWSs) based on critical slowing down. EWSs are derived from stochastic trajectories generated via Monte Carlo simulation with the Gillespie algorithm, incorporating intrinsic noise. It is shown that EWSs are more effective in capturing transitions from $M1 \rightarrow M1/M2$ and $M1/M2 \rightarrow M2$ than in detecting the direct transition from $M2 \rightarrow M1$.

25.

[Assessing the implications of morphine-induced dysregulation of autophagy on brain health](#)
JA Malik, JN Agrewala - Molecular Neurobiology, 2025

Abstract: Morphine has been a widely used drug for pain management and anesthesia in clinical settings for centuries and is also a drug of abuse. Its illicit use by individuals with substance use disorders has resulted in numerous brain-related complications. The immunopharmacology of morphine is highly complex, necessitating a deeper understanding of its interactions with brain regions involved in learning and memory. Autophagy is a conserved physiological recycling process that degrades cytoplasmic organelles and proteins, repurposing their components for cellular function. However, recent studies indicate that morphine exposure disrupts autophagic processes, contributing to many morphine-associated complications. This article highlights recent advancements in understanding the interplay between morphine and autophagy. By exploring this intricate relationship, we aim to enhance our knowledge of morphine-associated complications and autophagy dysregulation, potentially improving the management of morphine use disorder and related conditions, thereby promoting healthier outcomes.



[Beyond traditional time discretization: An efficient methodology for multidimensional weighted finite volume fragmentation equations](#)

S Yadav, D Wadhwa, M Singh, J Kumar - Physics of Fluids, 2025

26.

Abstract: Multidimensional population balance equations (MPBEs) model the dynamics of populations such as particles, cells, or droplets, considering properties like size, shape, liquid-to-solid ratio, and composition. Coupling MPBEs with computational fluid dynamics (CFD) enables the study of systems from micro to macro scales. However, the high dimensionality of MPBEs poses significant computational challenges. This paper presents a novel semi-analytical approach to address these challenges by approximating multidimensional weighted finite volume breakage PBEs [Saha et al. “Numerical solutions for multidimensional fragmentation problems using finite volume methods,” Kinet. Relat. Mod. 12(1), 79–103 (2019)]. The existing weighted finite volume scheme (WFVS) relies on the fourth-order Runge–Kutta method for solving discretized ordinary differential equations, where accuracy depends on grid type and the number of cells. The proposed approach eliminates the need for a time discretization, offering a more efficient alternative to traditional schemes. The time-free discretization nature of this method ensures seamless integration with CFD tools. To assess its effectiveness for two-dimensional (2D) and three-dimensional (3D) PBEs, nine combinations of selection functions, breakage kernels, and initial conditions are considered. As analytical solutions for the number density functions are unavailable, validation is performed using zeroth- and first-order integral moments. Results show that the new approach maintains the accuracy of existing methods while significantly improving computational efficiency—reducing runtime by approximately 60% for 2D PBEs and 80% for 3D PBEs. This efficiency makes the proposed approach a promising option for CFD applications.

[Calcium phosphate apatite filament co-wrapped with perforated electrospun sheet of phosphorylated chitosan—A bioinspired approach toward bone graft substitute](#)

P Dadhich, P Pal, N Dogra, PK Srivas, B Das, S Das, P Datta, B Saha, B Su, S Dhara - Journal of Biomedical Materials Research Part B: Applied Biomaterials, 2025

27.

Abstract: Bioinspired bone graft substitutes hold incredible opportunities in tissue engineering, potentiating the healing aspect. Here we have fabricated stacks of glutaraldehyde-genipin

	<p>crosslinked, microporous nanofibrous N-methyl phosphonic chitosan sheets (NMPC) with impregnated eggshell-derived CaP fibers to mimic osteonal architecture. This composite 3D rolled eggshell-derived calcium phosphate (ESCAP) scaffold (RCS), with density and modulus variation from the center to the periphery, has superior mechanical strength. The zwitterionic nature of NMPC, following the surface modulus of the CaP fibers, upgraded the biological performance. The low modulus of the flexible micro-perforated nanofibrous sheet increases along the ceramic phase, which prompts migration and distribution of proliferated MSCs from the outer polymeric surface to the inner ceramic region through micro-perforations. This movement stimulates endochondral ossification, observed by a gradual increment of collagen II expression alongside a decrement of collagen I expression. In vivo assessment of rabbit tibia bone defects revealed prominent healing in the presence of a scaffold by Day 60, accompanied by scaffold resorption. The cellular activity during healing revealed osteoblasts, osteocytes, blood vessels, and chondroblast cells at the boundary of the scaffolds, indicating neotissue and hypertrophic cartilage formation. Thus, the RCS bone grafts promote faster bone healing by osteogenesis and bone remodeling.</p>
28.	<p><u>Can intermittent teriparatide facilitate supraphysiological-rate distraction osteogenesis? A feasibility study in the rabbit tibial lengthening model</u> S Sharma, J Khing, N Kumar, R Naresh, P Sihota, MS Dhillon, S Aggarwal, P Sudesh - Indian Journal of Orthopaedics, 2025</p> <p>Abstract:</p> <p>Background</p> <p>Intermittent teriparatide administration is known to accelerate and promote bone healing. We wanted to investigate if intermittent teriparatide administration could facilitate supraphysiological-rate distraction osteogenesis (DO) in the rabbit tibial lengthening model without compromising on the regenerate quality.</p> <p>Methods</p> <p>24 New Zealand white rabbits underwent tibial lengthening of 10 mm by distraction osteogenesis and were divided into two groups. Group A ($n = 12$) underwent DO at the physiological (standard) rate of 0.75 mm per day and Group B ($n = 12$) underwent DO at the supraphysiological (accelerated) rate of 1.5 mm per day. Subgroups A1 and B1 received intermittent teriparatide, whereas subgroups A2 and B2 received saline as the vector control. The latency period (7 days) was equal in both groups. The consolidation phase was 2.5 times the distraction phase. Outcome parameters included mortality, number of failures of DO, regenerate volume, bone mineral density and strength of the regenerate as determined by the three-point bending test parameters (stiffness, work to failure and ultimate load to failure).</p> <p>Results</p> <p>There was one mortality in each group. Failure of distraction osteogenesis was noted in one animal in groups A1, A2 and B1, and four animals in Group B2. Kaplan–Meir survival analysis revealed significantly higher failures in Group B2 (log-rank test P value = 0.02). ANOVA revealed significant difference in regenerate stiffness ($P = 0.04$) among the four groups. However, the total volume, bone mineral density, work to failure and ultimate load to failure parameters were not significantly different among the four groups.</p> <p>Conclusion</p> <p>This feasibility study provides proof of concept of using teriparatide to accelerate distraction osteogenesis to supraphysiological levels, without compromising on the regenerate quality.</p>

[Carbon nanotube grafting for better electromagnetic shielding with carbon fiber/epoxy composites](#)
H Gupta, PK Agnihotri, S Basu, N Gupta - Polymer Composites, 2025

29.

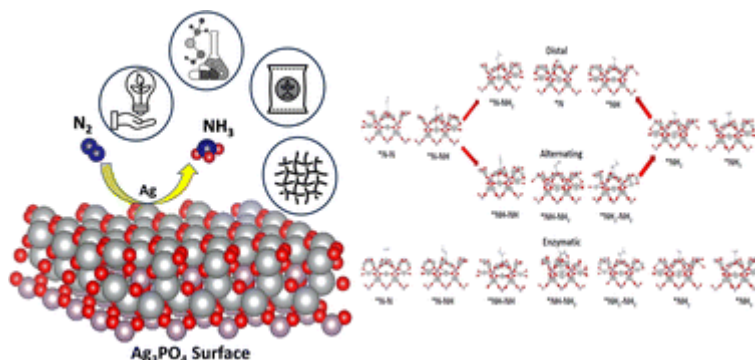
Abstract: Carbon fiber reinforced polymer (CFRP) composites are rapidly substituting metals as load-bearing structural components in space and defense applications. While their mechanical properties are sufficiently high, their capability to shield electromagnetic radiation needs improvement to meet current and future requirements. We demonstrate a novel method of enhancing the electromagnetic interference (EMI) shielding capability of conventional CFRP. We have grafted carbon nanotubes (CNTs) directly onto the surface of carbon fiber fabric using chemical vapor deposition (CVD) technique before incorporating them into the composite. The efficacy of this approach is assessed by comparing the DC electrical conductivity and EMI shielding effectiveness of CNT grafted CFRP with conventional CFRP. CNT-grafted CFRP laminates show significant improvement in anisotropic electrical conductivity: σ_x (along fiber length) by 150%, σ_y (transverse to the fiber length) by 407%, and σ_z (through-the-thickness) by 476%, relative to conventional CFRP. The increase in electrical conductivity improves the EMI shielding capabilities of CNT grafted CFRPs significantly. Moreover, the relative improvement in the EMI shielding performance is direction-dependent with better shielding performance when fibers are aligned with the incident electric field. EMI shielding effectiveness of CNT-grafted CFRP laminates increases by 30% (≈ 55 dB) at 8.75 GHz relative to the conventional CFRPs. Finally, it is shown that CFRP laminates with grafted carbon fibers perform much better than laminates when CNTs are added as a filler to the epoxy.

[Charge transfer and reaction coordinate construction based theoretical investigation of eNRR and HER on cuboidal silver phosphate: A tale of two competing mechanisms](#)

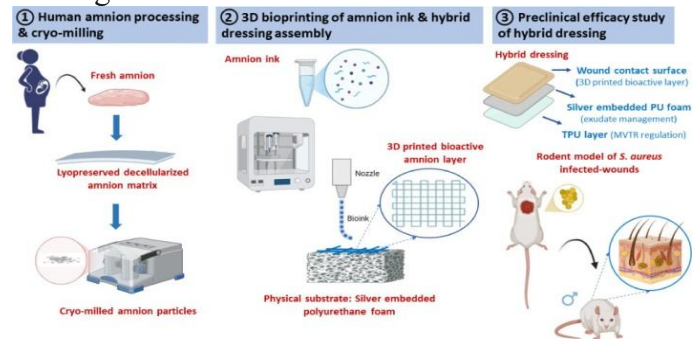
PP Mohanty, T Das, R Ahuja, S Chakraborty - Sustainable Energy & Fuels, 2025

30.

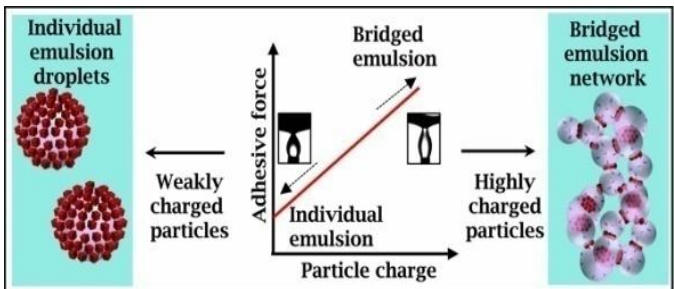
Abstract: We have performed systematic electronic structure calculations based on reaction coordinate construction and charge transfer analysis to explore the demarcation between two-competing mechanisms: the electrochemical nitrogen reduction reaction (eNRR) and hydrogen evolution reaction (HER). We have employed density functional theory based first-principles calculations to investigate the eNRR and HER on the cuboidal silver phosphate Ag_3PO_4 surface in an acidic medium. For the eNRR, we have explored all three reaction mechanism pathways named distal, alternating and enzymatic, while the adsorption site selectivity has also been envisaged in this work. Among all the possible catalytic sites of Ag_3PO_4 , the Ag site turned out to be the most energetically favourable for the eNRR that suppresses HER activity. The alternating pathway is confirmed to be the best catalytic pathway with a limiting potential of -0.60 V, as compared to -1.4 V and -2.9 V for distal and enzymatic pathways, respectively. The quantitative and qualitative analyses of the charge transfer process corresponding to the alternating pathway of the eNRR are also being explored from the perspective of Bader charge variation and charge density distribution.



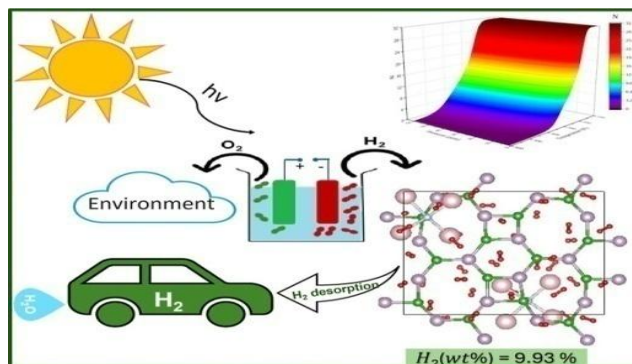
31.	<p><u>Chronic administration of morphine provokes generation of antibodies to morphine and immunosuppression in individuals with opioid use disorder</u> S Nanda, MA Zafar, S Singh, JA Malik, R Gautam, A Ghosh, D Basu, JN Agrewala - Journal of Biosciences, 2025</p> <p>Abstract: Globally, opioid use disorder (OUD) presents a significant public health challenge linked to high mortality and disability rates. Heroin and other morphine derivatives are prevalent among abused opioids. Prolonged exposure to these substances in individuals with OUD can trigger an immune response, leading to the production of antibodies to morphine that may bind to morphine and potentially mitigate its rewarding effects. In our study, we analyzed serum samples from patients diagnosed with OUD to explore the nature and properties of antibodies to morphine, aiming to characterize the generation of antibodies to morphine due to long-term exposure to morphine. We observed varying titers of antibodies to morphine in OUD patients, absent in healthy controls, with both free morphine and morphine complexes detected bound to these antibodies, indicating less potency. Furthermore, our analysis revealed elevated levels of FoxP3, a critical transcription factor in regulatory T-cells (Tregs) responsible for maintaining immunosuppression. Concurrently, reduced levels of inducible nitric oxide synthase (iNOS) and interleukin-6 (IL-6) indicated immunosuppressive activity. Notably, decreased antibody titers against the Acr1 protein of Mycobacterium tuberculosis suggested that morphine-induced immune suppression might compromise responses to other pathogens. These findings indicate that chronic morphine exposure not only suppresses host immunity but also induces the production of antibodies to morphine. Investigating whether these antibodies contribute to immune suppression or can be harnessed to combat morphine dependence presents an intriguing avenue for future research.</p>
32.	<p><u>3D Printed human amnion-based bioactive hybrid dressings for effective management of complex infected wounds</u> S Sarkar, AP Choudhari, A Mukherjee, V Rathi, B Das, AA Poundarik - ACS Applied Materials & Interfaces, 2025</p> <p>Abstract: Chronic wounds are often afflicted with persistent infection, excessive exudate accumulation, and delayed healing, leading to prolonged hospitalization. Excess moisture overhydrates the wound, promotes infection, and causes edema. Peri-wound skin may develop rashes, immersion injuries, and epidermal detachment. Nutrient-rich exudates foster microbial growth, increasing the infection risk. High bacterial loads lead to crust formation, continuous leakage, and foul odor, further complicating healing. To address this challenge, we developed a 3D printed amnion-based hybrid dressing comprising a regenerative layer integrated with a laminated silver-embedded polyurethane foam layer for partial and full thickness (thickness 0.12 mm–4 mm) infected wounds and burns. This dressing can suffice the varied clinical requirements of wound management by augmenting tissue regeneration, reducing bacterial load, and managing wound exudate. Human amnion was processed through decellularization and lyopreservation. Key angiogenic growth factors VEGF-A (54.12 ± 2.31 pg/mg) and PDGF-BB (3.760 ± 0.14 pg/mg) were quantified. Long-term in vitro cell viability was assessed for 20 days (as per ISO 10993–5 standards). Bioink was formulated using cryo-milled amnion particles and excipients optimized through rheology. Hybrid dressing was developed using an extrusion-based 3D printer, layering the amnion bioink onto the physical substrate, followed by lyophilization and gamma sterilization. Preclinical efficacy was assessed using a rodent Staphylococcus aureus-infected wound model, comparing the hybrid dressing to an in-house-developed amnion-mupirocin (AM) powder formulation with standard of care dressing. Both treatments demonstrated comparable wound closure rates and a significant bacterial load reduction. However, hybrid dressing offered superior healed tissue quality, increased CD31 expression, and improved neovascularization compared to AM powder treatment with a temporally regulated CD31 expression pattern mirroring the natural healing progression. This can be attributed to the hybrid construct of the dressing that provides</p>

	<p>effective exudate management, preventing its accumulation that could otherwise hinder angiogenesis, along with replenishment of wound bed with regenerative factors, aiding in mimicking the natural healing cascades.</p> 
33.	<p>Design approaches of high-entropy alloys using artificial intelligence: A review NM Eldabah, A Pratap, A Pandey, N Sardana, SS Sidhu, MAH Gepreel - <i>Advanced Engineering Materials</i>, 2025</p> <p>Abstract: This review explores the complex process of designing high-entropy alloys by combining theoretical guidelines, thermodynamic characteristics, and several modeling tools, including artificial intelligence approaches. It tackles issues in the design of high-entropy alloys, emphasizing the wide composition range, difficulty in forecasting phase stability, and requirement for specialized production techniques. The investigation expands on strategies for creating high-entropy alloys, emphasizing their benefits and limitations. This article discusses machine learning applications for predicting elastic characteristics, as well as the accompanying challenges and solutions. The future scenario predicts a collaborative world in which machine learning plays a critical role in the data-driven alloy design of high-entropy alloys, emphasizing ethical considerations and continual experimental validation for practical advances across industries.</p>
34.	<p>Development of an antibacterial Biginelli-based metal–organic nanocomposite-coated cotton fabric B Shah, N Singh, DO Jang - <i>Emergent Materials</i>, 2025</p> <p>Abstract: Pathogenic microorganism drug resistance has become a global health problem that is driving the development of novel antimicrobial materials. Metal–organic nanocomposites that operate through synergy offer a promising solution in this context. In this study, we synthesized substituted dihydropyrimidinone derivatives from substituted aromatic aldehydes, urea, and ethyl acetoacetate using a one-pot multicomponent Biginelli reaction. The antimicrobial potential of metal nanoparticles, particularly silver nanoparticles, is well-documented, and the antibacterial properties of dihydropyrimidinone derivatives are also well established. Hence, we combined the prepared Biginelli compounds with silver nanoparticles to form metal–organic nanocomposites that were subsequently screened for their antibacterial activities. The ABS-H2 nanocomposite exhibited concentration- and time-dependent behavior against <i>Escherichia coli</i> and <i>Staphylococcus aureus</i>. Finally, cotton fabric was endowed with antibacterial properties by applying this nanocomposite.</p>
35.	<p>Dynamics of light localization via coherent control: The interplay of transmission, absorption and disorder in photonic crystals N Ghangas, S Dasgupta, G Remesh, VG Achanta - <i>Optics Communications</i>, 2025</p> <p>Abstract: This study investigates the interplay between structural disorder, absorption, and Lyapunov exponent dynamics to exploit localization phenomena in photonic crystals with engineered defect layers. We generate disorder by introducing random refractive index variations in one of the bilayers, while the application of a control field to Λ-type atoms within a central defect layer enables dynamic tuning of the crystal's effective refractive index. We have employed</p>

	<p>traditional transfer matrix method to demonstrate transmission, Lyapunov exponents and absorption in the crystal. Through coherent control, we dynamically tune absorption, revealing sharp contrasts in band gap and band edge regions. while Lyapunov exponents, quantifying localization lengths, exhibit a consistent scaling across both band gap and band edge frequencies, and this behavior remains robust even in the presence of disorder. Hence, distinct localization mechanisms emerge at bandgap and band-edge frequencies. Bandgap localization arises from optical mode confinement and resonant alignment of atomic transitions with the probe field while band edge localization stems from a synergy of loss-difference-induced trapping and Anderson-like disorder effects. Notably, while disorder weakens confinement localization in the band gap, it actually strengthens localization at the band edges. These results deepen the understanding of light-matter coupling in disordered photonic systems and provide a framework for designing reconfigurable optical devices with tailored localization properties.</p>
36.	<p><u>Effect of distal fragment length on construct stability in an extra-articular distal tibial Fracture model fixed with locked intramedullary nailing: A biomechanical study</u> N Chauhan, S Kumar, T Thami, N Kumar, S Prabhakar, M Dhillon, S Sharma - Cureus, 2025</p> <p>Abstract: Introduction Fractures of the distal tibia are complex injuries with high complication rates, which include delayed union, non-union, and wound complications like dehiscence and infection. The two commonly employed definite internal fixation modalities include locked intramedullary (IM) nailing and plating. There is controversy regarding the superiority of the fixation construct, although nailing is proven to be more biological and devoid of soft tissue complications. There is also no consensus regarding the minimum distance of the fracture from the tibial plafond that is amenable to nailing of the fracture. Hence, the present study is designed to evaluate the effect of distal fragment length relative to the total length of the tibia, which makes it stable enough for IM nailing to be effective.</p> <p>Methods A prospective biomechanical study was performed using 28 fourth-generation composite tibial sawbones. Osteotomies were created at 12%, 15%, 20%, and 25% of the total tibial length (38 cm) from the distal articular surface, forming four experimental groups (A-D, n=7 each). All models were stabilized with 10 mm stainless-steel interlocking nails. Mechanical testing was conducted using a servo-hydraulic fatigue testing machine and included mediolateral (ML) and anteroposterior (AP) three-point bending, as well as cyclic axial loading. Outcome measures included bending stiffness, construct laxity (neutral zone), fracture gap angle, axial micromotion, and construct failure.</p> <p>Results The bending stiffness of all constructs tended to be lower in the AP plane than in the ML plane. The neutral zone of all groups tended to be higher in the AP plane than in the ML plane. The peak fracture gap angle tended to be higher in the AP plane than in the ML plane. Group A (shortest distal fragment length) demonstrated significantly lower AP stiffness, higher AP neutral zone, and higher AP peak fracture gap angle as compared to group D (longest distal fragment length). Group A demonstrated significantly greater instability in the AP plane than Group D. No statistically significant difference was found in the stability parameters on medio-lateral three-point bending and axial compressive testing.</p> <p>Conclusion</p>

	<p>The results of this biomechanical study show that comminuted extra-articular distal tibial fractures showsignificant instability in the sagittal plane when the length of the distal fragment is 12% of the total tibial length.</p>
37.	<p>Effect of particle surface charge and adhesive force on emulsion droplets bridging M Tiwari, M Sabapathy, VR Dugyala - Colloids and Surfaces A: Physicochemical and Engineering Aspects, 2025</p> <p>Abstract: This study is the first to demonstrate that emulsion droplets bridging and their coverage are strongly governed by the surface charge of particles and the adhesive force between particles and the dispersed phase. In this regard, the emulsions are prepared by in-situ surface modification of hematite particles by oleic acid in a water-decane medium at different salt concentrations and pH to tune the particle surface charge. The weakly charged particles stabilize fully covered emulsions, while highly charged particles formulate bridged emulsions. These observations are found consistent with a variety of oil-modifier systems. It has been determined, the stabilization of bridged emulsion cannot be solely attributed to particle wettability and surface charge. Therefore role of adhesive force in dependence on particle surface charge is investigated with the help of droplet stretching experiments in different salinity/pH conditions. The adhesive force is calculated by applying force balance across the bridged area of the oil droplet and particle-laden oil–water interface, in the stretching experiment. The results show that the adhesive force is stronger between the highly charged particles–oil phase compared to the weakly charged particles–oil phase, regardless of the type of oil-modifier system. This variation in adhesive force is considered as an attribution of electrostatic interaction between particle and modifier at the interface. Accordingly, a master curve is provided by normalizing adhesive force by surface force, which shows adhesive force should be at least 0.7 times the surface force to design such bridged emulsion with any type of system.</p> 
38.	<p>Efficient hydrogen storage in superalkali NLi₄-decorated boron phosphide biphenylene D Dange, P Beniwal, TJ Dhillip Kumar - ACS Applied Energy Materials, 2025</p> <p>Abstract: Two-dimensional porous materials are potential candidates for reversible hydrogen storage. Driven by the growing popularity of organic biphenylene materials, we explored the hydrogen storage capacity of superalkali NLi₄-decorated boron phosphide biphenylene (BPB) using first-principles calculations employing the GGA-PBE functional enhanced with van der Waals corrections. Interestingly, NLi₄ was strongly bonded with the BPB monolayer via an electronic charge transfer mechanism with a large binding energy of -5.38 eV when decorated on one side and -5.34 eV/NLi₄ when decorated on both sides of the monolayer. The NLi₄@BPB complex can adsorb up to 16 H₂ molecules, and the 2NLi₄@BPB complex adsorbs a maximum of 32 H₂ molecules with the H₂ adsorption energy ranging from -0.35 to -0.24 eV/H₂, resulting in a hydrogen storage capacity of 5.6 and 9.93 wt %, respectively, surpassing the DOE target of 5.5 wt %. H₂ interacts with Li atoms in NLi₄ clusters by charge polarization, which causes lengthening of the H–H bond. The hydrogen occupation index evaluated for various temperatures and pressures reveals, about the hydrogen reversibility, that the material offers complete desorption above 380 K at 1 atm. Ab initio molecular dynamics simulations further confirm the structural stability and the</p>

reversibility of hydrogen adsorption. From the findings, NLi₄-decorated BPB proved to be a very efficient hydrogen storage material.

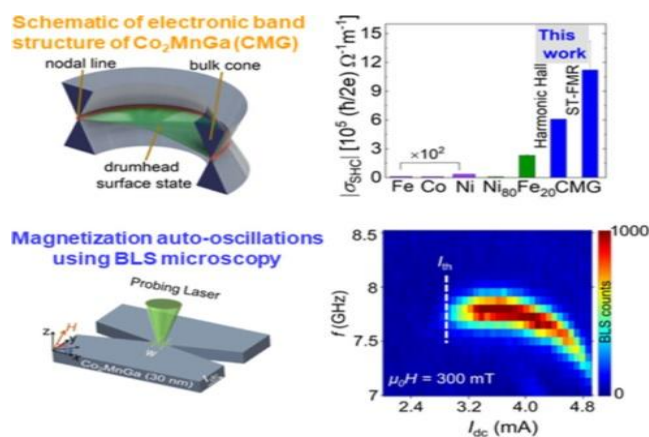


Energy-Efficient single layer spin hall nano-oscillators driven by berry curvature

L Bainsla, Y Sakuraba, A Kumar, AK Chaurasiya, K Masuda, N Suwannaharn, AA Awad, N Behera, R Khymyn, T Sasaki, SP Dash, J Åkerman - ACS nano, 2025

39.

Abstract: Spin Hall nano-oscillators (SHNOs) are emerging spintronic oscillators with significant potential for technological applications, including microwave signal generation, and unconventional computing. Despite their promising applications, SHNOs face various challenges, such as high energy consumption and difficulties in growing high-quality thin film heterostructures with clean interfaces. Here, single-layer topological magnetic Weyl semimetals open a possible solution as they possess both intrinsic ferromagnetism and a large spin–orbit coupling due to their topological properties. However, producing such high-quality thin films of magnetic Weyl semimetals that retain their topological properties and Berry curvature remains a challenge. We address these issues with high-quality single-layer epitaxial ferromagnetic Co₂MnGa Weyl semimetal thin film-based SHNOs. We observe a giant spin Hall conductivity, $\sigma_{\text{SHC}} = (6.08 \pm 0.02) \times 10^5 (h/2e) \Omega^{-1} \text{m}^{-1}$, which is an order of magnitude higher than previous reports. Theoretical calculations corroborate the experimental results with a large intrinsic spin Hall conductivity due to presence of a strong Berry curvature. Further, self spin-orbit torque driven magnetization auto-oscillations are demonstrated for the first time, at an ultralow threshold current density of $J_{\text{th}} = 6.2 \times 10^{11} \text{A m}^{-2}$. These findings indicate that magnetic Weyl semimetals have tremendous application potential for developing energy-efficient spintronic devices.

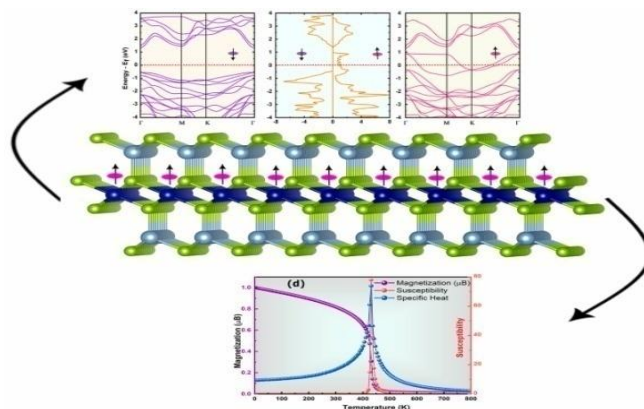


Engineering of two-dimensional half-metallic CoAl₂Se₄ with intrinsic ferromagnetism and high Curie temperature

40.

H Lahraichi, M Kibbou, Z Haman, S Bouhou, I Essaoudi, **R Ahuja**, A Ainane - Computational Materials Science, 2025

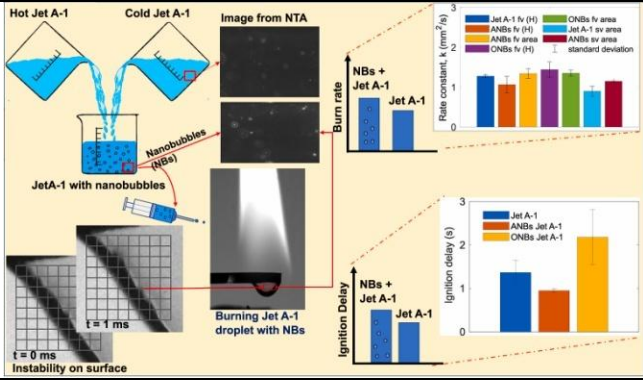
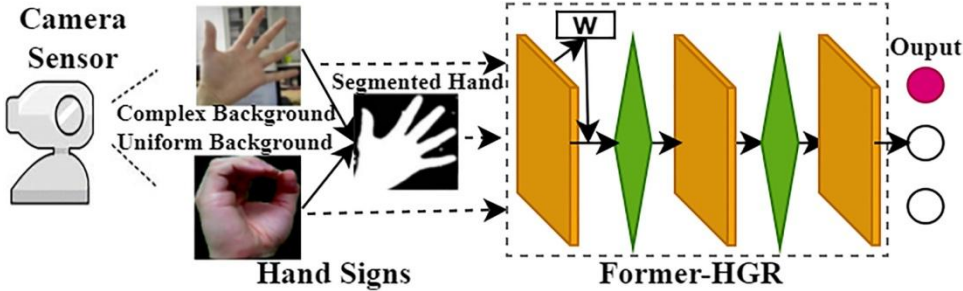
Abstract: Half-metallic magnets with high Curie temperatures (T_c) are essential for the advancement of next-generation spintronic technologies. In this study, we perform a comprehensive first-principles investigation of the CoAl_2Se_4 monolayer, an AM_2X_4 -type material that has remained largely unexplored. Our findings confirm its energetic, mechanical, and dynamical stability, as evidenced by cohesive and formation energy calculations, elastic constants, and phonon dispersion analysis. The observed ferromagnetic behavior arises from Co-Se-Co bond superexchange interactions, in agreement with the Goodenough–Kanamori rules. The monolayer exhibits robust half-metallicity, characterized by a substantial half-metallic gap of 2.76 eV, enabling fully spin-polarized electronic conduction. Magnetic anisotropy energy calculations indicate an easy-plane magnetization, while Monte Carlo simulations predict a high Curie temperature of 431 K, well above room temperature, ensuring stable magnetic ordering under ambient conditions. These outstanding properties position the CoAl_2Se_4 monolayer as a promising candidate for spin filtering devices, magnetoresistive sensors, and next-generation magnetic memory technologies.



[Experimental studies on the effect of bulk nanobubbles on the combustion of Jet A-1](#)
V Kurumanghat, H Sharma, N Nirmalkar, L Kabiraj - Fuel, 2025

Abstract: Over the last two decades, nanobubbles (NBs) have demonstrated remarkable long-term stability, allowing them to retain gas in liquids. In this work, the interest is to achieve control over the combustion performance of liquid fuels by infusing bulk NBs into Jet fuel. The generation of air bulk nanobubbles (ANBs) and oxygen bulk nanobubbles (ONBs) in Jet A-1 is performed, and their effect on the combustion of Jet A-1 droplets is investigated. Bulk NBs were generated in Jet A-1 by the hot and cold solvent mixing method. Generated bulk NBs were characterized by a nanoparticle tracking analyzer and ZetaSizer to get their concentration, diameters, and zeta potential. High-speed imaging of single droplet combustion of nanobubble-infused Jet A-1 is studied to estimate droplet burn rate and ignition delay. The results show that the bulk NBs were stable over a period of 30 days. The combustion experiment shows that the droplets of ONBs containing Jet A-1 burned faster than pure Jet A-1 droplets. Nanobubble-incorporated Jet A-1 droplets exhibit surface instabilities during droplet combustion. Additionally, the presence of ANBs and ONBs affects the ignition delay of Jet A-1 droplets, which reveals that the type of gas present in the bulk NBs influences ignition delay.

41.

	 <p>The figure illustrates the experimental setup and results for nanobubble-assisted combustion. It shows the process of creating nanobubbles (NBs) in Jet A-1 fuel using both hot and cold jets. The resulting Jet A-1 with nanobubbles is shown in a beaker. The burning Jet A-1 droplet with NBs is shown in a micrograph. The figure also includes NTA (Nanotracking Analysis) images and graphs showing the burn rate and ignition delay for Jet A-1 and Jet A-1 with NBs. The burn rate graph shows that the burn rate is higher for Jet A-1 with NBs compared to Jet A-1. The ignition delay graph shows that the ignition delay is lower for Jet A-1 with NBs compared to Jet A-1.</p>
42.	<p>Former-HGR: Hand gesture recognition with hybrid feature-aware transformer M Verma, G Gopalani, S Bharara, SK Vipparthi, S Murala, M Abdel-Mottaleb - IEEE Sensors Letters, 2025</p> <p>Abstract: Hand Gesture Recognition (HGR) systems, using cameras and sensors, offer an intuitive method for human-machine interaction, sparking interest across various applications. However, these systems face challenges from environmental factors like variations in illumination, complex backgrounds, diverse hand shapes, and similarities between different gesture classes. Achieving accurate gesture recognition under such conditions remains a complex task, necessitating robust solutions to ensure reliable performance. This letter proposes a novel approach named Former-HGR, a hybrid feature-aware transformer for HGR. Unlike traditional transformer-based HGR systems that heavily rely on computationally intensive self-attention mechanisms, Former-HGR enhances global feature perception by applying self-attention across channels through the integration of Multi-Dconv Head Transposed Attention (MDTA). Additionally, Former-HGR improves feature extraction by incorporating multi-scale features and effectively filters redundant information using a Hybrid Feature-Aware Network (HFAN). Extensive experiments conducted on three data sets: NUSII, OUHANDS, and MUGD, demonstrate that Former-HGR outperforms recent benchmark HGR approaches, achieving accuracy improvements of up to 14% in person-independent validation schemes.</p>  <p>The diagram illustrates the Former-HGR architecture. It starts with a Camera Sensor capturing images of a hand against both a complex background and a uniform background. These images are processed to produce a Segmented Hand and Hand Signs. The Segmented Hand is then fed into the Former-HGR network, which consists of a series of blocks (W, green diamonds, orange rectangles) leading to an Output.</p>
43.	<p>Frobenius numbers associated with Diophantine triples of $x^2+3y^2=z^3$ T Komatsu, T Chatterjee - Revista de la Real Academia de Ciencias Exactas, Físicas y Naturales. Serie A. Matemáticas, 2025</p> <p>Abstract: We give an explicit formula for the p-Frobenius number of triples associated with Diophantine equations $x^2+3y^2=z^3$, that is, the largest positive integer that can only be represented in at most p many ways by combining the three integers of the solutions of Diophantine equations $x^2+3y^2=z^3$.</p>
44.	<p>Harnessing phase-dependent acidity and redox activity of ru-decorated CePO₄ catalysts for biofuel production from lignin model compounds and lignin bio-oil A Kumar, R Srivastava - ACS Sustainable Chemistry & Engineering, 2025</p>

Abstract: Lignin valorization offers a sustainable route to biofuel production, addressing global energy demands and environmental concerns. In this study, Ru-decorated cerium phosphate (CePO_4) catalysts with distinct crystalline phases (hexagonal, monoclinic, and mixed) were synthesized to investigate the influence of phase-dependent properties on catalytic transfer hydrogenation (CTH) of phenethyl phenyl ether (PPE), a lignin model compound, and catalytic hydrogenation of lignin bio-oil derived from softwood biomass into cycloalkanes. The hexagonal phase ($\text{CePO}_4\text{-H}$) emerged as the most effective support, offering superior Lewis/Bronsted acidity, redox activity ($\text{Ce}^{3+}/\text{Ce}^{4+}$), and Ru nanoparticles dispersion. The $\text{Ru}(2\%)/\text{CePO}_4\text{-H}$ offered 99% conversion under CTH conditions, selectively cleaving $\beta\text{-O-4}$ ether linkages in PPE to produce ethylbenzene and cyclohexanol as the sole products under mild conditions (150°C , 6 h, 1 MPa N_2). The catalyst afforded a near-quantitative yield of saturated cyclic hydrocarbons from PPE under catalytic hydrogenation conditions (150°C , 6 h, 1 MPa H_2). Furthermore, $\text{Ru}(2\%)/\text{CePO}_4\text{-H}$ offered nearly complete conversion (99%) of lignin bio-oil into fully saturated cyclic $\text{C}_6\text{-C}_9$ products (suitable for aviation fuel applications) with up to 99% selectivity under catalytic hydrogenation conditions (220°C , 3 MPa H_2). Mechanistic insights revealed that the enhanced catalytic performance arises from phase-dependent surface acidity, electron-enriched Ru^0 sites, and strong metal-support interactions, facilitating efficient C–O bond cleavage and hydrodeoxygenation/hydrogenation of PPE. The green chemistry metrics further substantiate the reduced environmental impact of this catalytic process. This work highlights the transformative potential of phase-engineered $\text{Ru}(2\%)/\text{CePO}_4\text{-H}$ catalysts for lignin bio-oil upgrading. It provides a blueprint for designing robust catalysts with tunable properties for scalable, sustainable biofuel production.

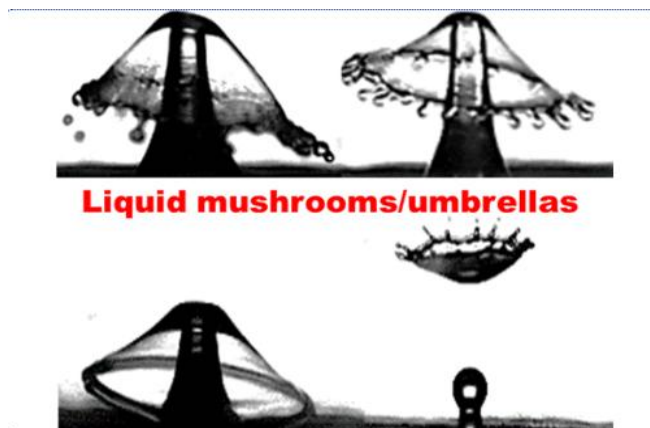


45.

Hydrodynamics of liquid mushrooms

AM Bhaskaran, A Paul, A Roy, D Samanta, P Dhar - Langmuir, 2025

Abstract: Droplets that impact upon the free surface of a liquid pool may generate a vertically rising jet after the cavity formation and collapse events, provided the droplet has sufficient kinetic energy at impact. Depending on the associated time scales and the effect of the Rayleigh-Plateau instability, the jet may either continue to rise upward as a whole or may form satellite droplets via necking of the jet tip. Collision of these structures (either the jet or the secondary droplets) with a second identical incoming droplet, ejected from the same dispensing source as the first one, may result in the formation of various lamellar or domed fluid structures, and depending on the impact conditions, give rise to liquid mushrooms and/or umbrellas. In this research, we experiment with the hydrodynamics of such liquid mushrooms and study the effects of droplet impact velocity, fluid surface tension, and viscosity on the behavior of such lamellar structures. The role of surface tension and viscosity in the dynamics, evolution, and longevity of the mushrooms is studied. We further explore the role of the orientation of incoming droplet impact, i.e., whether head-on or offset collision with the rising jet/satellite droplet. We discuss the spatiotemporal evolution of the mushroom diameters and its susceptibility to surface tension, viscosity, and droplet impact velocity (release height). We put forward a theoretical model based on energetics to predict the maximum spread diameter of the lamellae, and it yields accurate predictions. Our findings may help to provide important insights into a fluid dynamic phenomenon observed in nature, studied extensively by artists and photography enthusiasts for its aesthetics, and may be important in certain niche utilities as well.

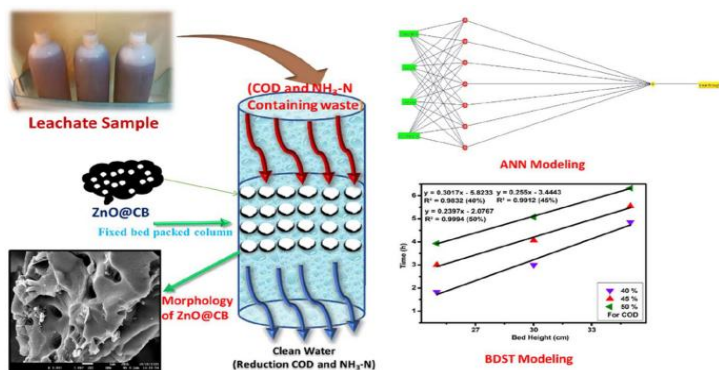


[Innovative use of immobilized zinc oxide-impregnated activated carbon \(ZnO@CB\) for effective treatment of leachate: modeling and predictive assessment](#)

K Singh, RK Lohchab, G Goel, **SA Waziri**, H Aguedal, Y Allab, MEAE Elmeliani, A Iddou, B Liu, M Terashima, S Kaswan - Environmental Science and Pollution Research, 2025

46.

Abstract: This study examined the viability of column method utilizing the immobilized zinc oxide-loaded activated carbon obtained from corncob (ZnO@CB) to treat the landfill leachate. Instrumental techniques like BET, FTIR, SEM–EDX, and XRD were applied for the characterization of the adsorbents. The break through curve (BTC) was evaluated by altering the flow rate, bed height, and initial concentration of $\text{NH}_3\text{-N}$ and COD. At 35 cm bed height with an initial level of 3264 mg-COD/L, the optimal adsorption capacity was observed to be 35.44 mg-COD/g. Meanwhile, the optimal $\text{NH}_3\text{-N}$ adsorption capacity was 4.81 mg- $\text{NH}_3\text{-N}$ /g at a flow @ 1 mL/min, with an initial concentration of 460 mg- $\text{NH}_3\text{-N}$ /L, and a bed height of 35 cm. Both $\text{NH}_3\text{-N}$ and COD adsorption exhibited a correlation coefficient higher than 0.98 as calculated by linear plots of bed depth service time (BDST) equations, indicating that the column structure model was appropriate. The results reveal that the performance of the adsorption process could be well predicted by artificial neural network (ANN) at 4, 7, and 1 neuron for input, middle, and output layers, with a mean absolute error of 0.0096 and 0.0093 for COD and $\text{NH}_3\text{-N}$ reduction, respectively. In the RF model, higher values of R^2 (0.9876 for COD and 0.9874 for $\text{NH}_3\text{-N}$) indicate the model accuracy. The regenerated adsorbent achieved 54.2% and 54.1% removal of

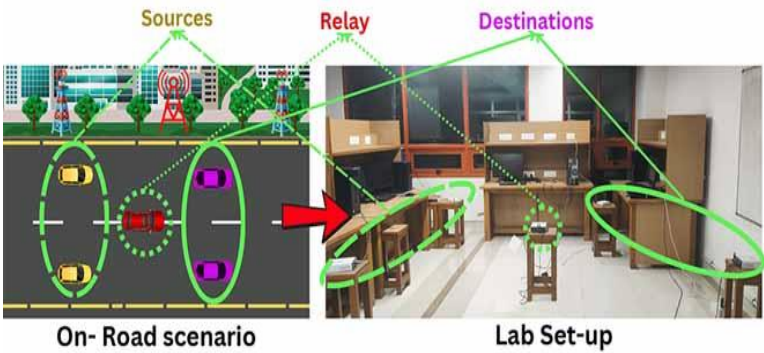
	<p>COD and $\text{NH}_3\text{-N}$ and adsorbent usage was feasible for up to three cycles. Results of BDST, ANN, and RF models revealed that packed column with immobilized ZnO@CB adsorbent is an efficient method for treating landfill leachate, highlighting the potential of ZnO@CB for industrial applications.</p> 
47.	<p><u>Intrinsic role of Lagrangian and Stokes drift owed to currents in a stratified three-layered channel with interfacial tensions</u> D Goyal, SC Martha - European Journal of Mechanics-B/Fluids, 2025</p> <p>Abstract: The present study analyses the trajectories of the fluid particles, Stokes drift and Lagrangian drift mechanisms for three-layered internal flow having two interfaces with interfacial tensions. The three-fluid layers are of different densities. A uniform and two dimensional current is flowing in each fluid layer. The pathline equations with first-order solution analysis produces closed trajectories. The trajectories of the fluid particles in the middle layer shows non-monotonic trend as it is subjected to two interfaces and get shorten according to the strength of density stratification and interfacial tensions. The analytical expressions for Stokes drift are found in each layer using small-excursion principle. Based on these expressions, we found that the variation in density causes the Stokes drift displacement to increase more robustly after a critical density ratio for both interfaces. The underlying mechanism of this behaviour is the phase reversal phenomenon which is analysed via phase plane analysis. The trajectories in spatial phase plane are open implying that Stokes drift occurs in each fluid layer. Moreover, the change in density ratio alters the direction of these open trajectories in middle layer at both interfaces, which are shown by drawing their directional fields. The expressions for Lagrangian drift which are dependent on density variations and interfacial tensions are analysed by the ratio of Eulerian return flow to the depth averaged Stokes drift at both interfaces. It is found that weak stratification with higher tension at interface lead to dominance of Eulerian return flow over averaged Stokes drift for middle layer. Also, the effect of these parameters are predominant in the intermediate wave regimes. These observations are essential for understanding the wave characteristics, sediment movement, anticipating the dispersal of contaminants, and modelling climate-related processes like the spread of heat and carbon. Therefore, the study of multilayer systems with Stokes and Lagrangian drift has a considerable potential to further our understanding of marine processes, especially in areas where internal wave action and substantial stratification are present.</p>
48.	<p><u>Iodine-mediated peptide disulfide bridging is reversible and sequence-dependent in solid support: Use of tempo in the reaction resolves the challenge</u> A Chowdhury, NM Tripathi, N Verma, S Ghosh, B Pati, A Bandyopadhyay - Asian Journal of Organic Chemistry, 2025</p> <p>Abstract: Iodine (I_2) is an extremely popular reagent for disulfide assembly in solution, solid phase (pseudo-dilute conditions) peptides, and immobilized materials. However, we noticed that I_2-mediated peptide disulfide assembly often resulted in incomplete reactions due to its redox activity under pseudo-dilute conditions. The phenomenon intrigued us to conduct an in-depth analysis of</p>

	<p>I₂-mediated disulfide assembly with various peptide sequences. We revealed that the redox equilibrium between free thiols and disulfide products was peptide sequence-dependent and previously unsolicited. Adding TEMPO in the reaction medium attenuates the I₂-mediated redox equilibrium and rapidly (~5 min) promotes quantitative, clean disulfide assembly. Finally, in silico investigations supported that this chemical equilibrium primarily relies with the increased global free energy upon macrocyclization and the interspace between thiol groups in the linear peptide chain. This fundamental study will leverage multiple advantages in disulfide formation in immobilized materials and peptide modification chemistries with iodine in solid support.</p>
49.	<p>Isovitexin, a natural adiponectin agonist, prevents glucocorticoid-induced osteosarcopenia C Kulkarni, S Kumar, S Khatoon, S Sadhukhan, KR Washimkar, A Kumar, S Sharma, S Rajput, K Porwal, MN Mugale, SK Rath, MM Godbole, S Sanyal, N Kumar, A Mithal, N Chattopadhyay - Endocrine, 2025</p> <p>Abstract:</p> <p>Purpose</p> <p>Isovitexin is an agonist of adiponectin receptors (AdipoRs). Adiponectin has been shown to have beneficial effects on bone and muscle function, in addition to its positive impact on metabolic health. However, the preclinical and clinical application of adiponectin faces scalability challenges, prompting the investigation of isovitexin in a methylprednisolone (MP)-induced osteoporosis model.</p> <p>Methods</p> <p>A rat model of MP-induced osteoporosis was developed to evaluate isovitexin's effects on bone health, including bone mass & microarchitecture (MicroCT), turnover markers (P1NP and CTX-1), strength (three-point bending, and nanoindentation), and quality (FTIR). We also investigated the muscle protective effects of isovitexin by measuring key muscle catabolic (atrogenes) proteins.</p> <p>Results</p> <p>Isovitexin effectively prevented MP-induced osteopenia in critical weight-bearing, fracture-prone sites, such as the proximal femur and lumbar vertebrae. Bone turnover markers revealed its osteogenic and anti-resorptive properties, crucial for countering glucocorticoid-induced bone loss. Isovitexin treatment preserved the mineral and material composition of bone, indicating that it helps maintain the tissue integrity and mechanical strength. Hitherto observed effects of isovitexin likely resulted in the preservation of bone quality, demonstrated by preserving mechanical behavior and bone strength, which are essential for preventing fractures. MP treatment led to muscle atrophy, evidenced by reduced gastrocnemius diameter and cross-sectional area. Isovitexin countered these effects and inhibited atrogenes (atrogin-1 and MuRF-1) induction.</p> <p>Conclusion</p> <p>Isovitexin not only mitigates osteopenia but also maintains overall bone quality and composition, exhibiting dual osteogenic and anti-resorptive effects. Its capacity to reduce muscle atrophy underscores its potential as a comprehensive treatment for glucocorticoid-induced osteoporosis and sarcopenia.</p>
50.	<p>Mapping of radionuclides for radiological impact assessment in cultivated soils of Punjab, India SS Kaintura, K Tiwari, S Devi, S Thakur, M Prasad, D Meena, PP Singh - Applied Radiation and Isotopes, 2025</p> <p>Abstract: This study investigates and maps the distribution of radionuclides and associated radiation hazards in soil specimens collected from the Ropar agricultural region, Punjab, India. A high-resolution HPGe detector was utilized to measure and assess radioactivity precisely. The</p>

	<p>specific activities of ^{226}Ra, ^{232}Th, and ^{40}K ranged from 34.15 to 122.36 Bq kg⁻¹, 58.24 to 176.77 Bq kg⁻¹, and 385.02 to 785.57 Bq kg⁻¹, respectively. Their average values, 49.43 ± 18.65 Bq kg⁻¹, 76.82 ± 28.88 Bq kg⁻¹, and 591.22 ± 105.68 Bq kg⁻¹, respectively, exceeded the corresponding global averages. The quantified radium equivalent averaged 204.65 ± 50.91 Bq kg⁻¹, remaining below the permissible limit of 370 Bq kg⁻¹ but considerably higher than the world average of 129.59 Bq kg⁻¹. All hazard and level indices were markedly lower than the permissible limit of unity. However, the gamma radiation dose rates (\dot{D}_{in} and \dot{D}_{out}), annual effective doses (A_{Din} and A_{Dout}), and associated cancer risk levels (ELCR_{in} and ELCR_{out}) for both indoor and outdoor environments exceeded the corresponding recommended levels. The contributions of individual radionuclides to radiological indices and gamma doses were analyzed, identifying ^{232}Th as the primary source of radiation exposure, while Correlations among radionuclides and hazard indices were analyzed to evaluate their interrelationships.</p>
51.	<p>Modeling dissipative magnetization exchange dynamics in magnetic resonance N Sehrawat, MK Pandey, R Ramachandran - Physical Chemistry Chemical Physics, 2025</p> <p>Abstract: Quantifying the role of the environment in a quantum system of interest has remained an active pursuit for studying the effects of dissipation in a wide-range of problems in chemical physics and spectroscopy. From an operational perspective, the complexities encountered in the description of open systems have ushered in the development of models without explicit consideration of the complete system. To this end, phenomenological descriptions that involve the inclusion of exponential damping terms have remained the method of choice. While such methods have gained prominence in providing a qualitative explanation for observations in spectroscopy, they are of limited utility in quantitative studies that involve the estimation of molecular constraints. As an alternative, the present report explores the possibility of understanding the nuances of dissipation found in open systems through analytic methods. Specifically, the magnetization exchange between a pair of spins (say I_1 and I_2) is examined under periodic modulation in the presence of a surrounding bath of other spins. Employing the concept of effective Hamiltonians and utilizing the block-diagonal structure of the derived effective Hamiltonians, analytic expressions are derived for describing the effects of dissipation (due to neighboring spins) on the system of interest without increasing the dimension of the problem.</p>
52.	<p>Non-relativistic conformal field theory in momentum space RK Gupta, Meenu - The European Physical Journal C, 2025</p> <p>Abstract: Non-relativistic conformal field theory describes many-body physics at unitarity. The correlation functions of the system are fixed by the requirement of the conformal invariance. In this article, we discuss the correlation functions of scalar operators in non-relativistic conformal field theories in momentum space. We discuss the solution of conformal Ward identities and express 2,3, and 4-point functions as a function of energy and momentum. We also express the 3- and 4-point functions as the one-loop and three-loop Feynman diagram computations in the</p>

	momentum space. Lastly, we generalize the discussion to the momentum space correlation functions in the presence of a boundary.
53.	<p>Non-symmetrical vortex beam shaping in VECSEL laser arrays S Karuseichyk, I Audoin, V Pal, F Bretenaker - Photonics Research, 2025</p> <p>Abstract: We propose and numerically test, to our knowledge, a novel concept for asymmetric vortex beam generation in a degenerate vertical external cavity surface emitting laser (DVECSEL). The method is based on a phase-locking ring array of lasers created inside a degenerate cavity with a binary amplitude mask containing circular holes. The diffraction engineering of the mask profile allows for controlling the complex coupling between the lasers. The asymmetry between different lasers is introduced by varying the hole diameters corresponding to different lasers. Several examples of masks with non-uniform or uniform circular holes are investigated numerically and analytically to assess the impact of non-uniform complex coupling coefficients on the degeneracy between the vortex and anti-vortex steady states of the ring laser arrays. It is found that the in-phase solution always dominates irrespective of non-uniform masks. The only solution to make one particular vortex solution dominant over other possible steady-state solutions consists of imprinting the necessary phase shift among neighboring lasers in the argument of their coupling coefficients. We also investigate the role of the Henry factor inherent to the use of a semiconductor active medium in the probabilities to generate vortex solutions. Analytical calculations are performed to generalize a formula previously reported [Opt. Express 30, 15648 (2022)], for the limiting Henry factor to cover the case of complex couplings.</p>
54.	<p>Ocular drug delivery systems based on nanotechnology: a comprehensive review for the treatment of eye diseases RD Bairagi, RR Reon, MM Hasan, S Sarker, D Debnath, MT Rahman, S Rahman, MA Islam, MAT Siddique, B Bokshi, MM Rahman, AK Acharzo - Discover Nano, 2025</p> <p>Abstract: Ocular drug delivery is a significant challenge due to the intricate anatomy of the eye and the various physiological barriers. Conventional therapeutic approaches, while effective to some extent, often fall short in effectively targeting ocular diseases, resulting in suboptimal therapeutic outcomes due to factors such as poor ocular bioavailability, frequent dosing requirements, systemic side effects, and limited penetration through ocular barriers. This review elucidates the eye's intricate anatomy and physiology, prevalent ocular diseases, traditional therapeutic modalities, and the inherent pharmacokinetic and pharmacodynamic limitations associated with these modalities. Subsequently, it delves into nanotechnology-based solutions, presenting breakthroughs in nanoformulations such as nanocrystals, liposomes, dendrimers, and nanoemulsions that have demonstrated enhanced drug stability, controlled release, and deeper ocular penetration. Additionally, it explores a range of nanosized carriers, including nano-structured lipid carriers, hydrogels, nanogels, nanoenzymes, microparticles, conjugates, exosomes, nanosuspensions, viral vectors, and polymeric nanoparticles, and their applications. Unique insights include emerging innovations such as nanowafers and transcorneal iontophoresis, which indicate paradigm shifts in non-invasive ocular drug delivery. Furthermore, it sheds light on the advantages and limitations of these nanotechnology-based platforms in addressing the challenges of ocular drug delivery. Though nano-based drug delivery systems are drawing increasing attention due to their potential to enhance bioavailability and therapeutic efficacy, the review ends up emphasizing the imperative need for further research to drive innovation and improve patient outcomes in ophthalmology.</p>
55.	<p>On the microstructure and mechanical behavior of AS-CAST, WIRE-ARC, and laser additively manufactured nickel-aluminum-bronze alloy MK Mishra, AG Rao, A Tripathi, D Singh, R Kumar - Metallography, Microstructure, and Analysis, 2025</p>

	<p>Abstract: The microstructure and mechanical behavior of nickel-aluminum-bronze alloy manufactured from different routes, such as laser additive manufacturing, wire-arc additive manufacturing, and conventional casting, have been investigated. Microstructural characterization using scanning electron microscope (SEM) showed significant variation in the microstructure. A finer structure was observed in wire-arc additively manufactured samples compared to the as-cast samples. κ_1 phase was not observed in additively manufactured samples. The highest tensile strength of 745 MPa was observed for the laser additive sample.</p>
56.	<p>Orbit by the up-down action of braid diagrams K Negi, A Shimizu, Y Yaguchi, M Prabhakar - Journal of Knot Theory and Its Ramifications, 2025</p> <p>Abstract: The set of all virtual or classical braid diagrams forms a monoid and gives a natural monoid action on a direct product of Z called the up-down action. In this paper, we determine the orbit of every tuple of Z under the up-down action of virtual or classical braid diagrams. Moreover, we determine the orbit for irreducible braid diagrams. We also consider the isotropy submonoid and give a condition for a braid diagram to admit an up-down coloring to its closure.</p>
57.	<p>Perception of healthcare providers and patients on Kalari marmachikilsa: an indigenous medical practice in India A Nandha, AV Suresh - Humanities and Social Sciences Communications, 2025</p> <p>Abstract: Kalari marmachikilsa (KMC) is an indigenous and natural medical practice that originated in ancient India. KMC employs the traditional Indian knowledge of marma points to treat not just the symptoms of a disease but the underlying cause of ailments. In traditional Indian medical texts, marmas are considered as vital energy points located in various parts of the human body housing energy or life force called prana. This study provides a novel investigation of the perceptions of the healthcare providers (HCPs) of KMC and the Kalari marmachikilsa patients (KMPs) being treated. The results provide data that supports the restoration of this relegated traditional Indian medical system and greater awareness of the potential of natural medical practices. A mixed method approach utilized in the study helps to comprehend and authenticate the validity of responses in qualitative and quantitative data. Insights from the data reveal information on the existing customs, convictions, therapeutic procedures, and overall knowledge related to this medical practice. Themes elicited from the responses provide a better understanding of the perception of participants on KMC. Through the interpretation of data, the study reveals the acceptability, affordability, and credibility of this treatment method according to its practitioners and patients. Perceptions of KMC demonstrate the benefits of availing this treatment method and reiterate the potential gains of reviving this traditional sustainable treatment method.</p>
58.	<p>Performance analysis of STAR-RIS aided short-packet NOMA network under imperfect SIC and CSI S Kumar, B Kumbhani, S Darshi - IEEE Systems Journal, 2025</p> <p>Abstract: Simultaneously transmitting and reflecting reconfigurable intelligent surface (STAR-RIS) and nonorthogonal multiple access (NOMA) are promising solutions for next-generation wireless networks with massive connectivity, ultra-low latency, ultra-high reliability, and spectral efficiency. This article analyzes the performance of the downlink STAR-RIS-aided short-packet (SP)-NOMA (STAR-RIS-SP-NOMA) network under the constraint of imperfect successive interference cancellation (ipSIC) and imperfect channel state information (ipCSI) by using a Nakagami-m fading environment. To characterize the system performance, first, we derive the statistical distribution of cascaded Nakagami-m channels using the Laguerre polynomial series approximation. Second, the approximate closed-form expressions in terms of average block error rate (ABLER), system throughput, goodput, latency, and reliability are derived. Third, the</p>

	<p>asymptotic analysis is also done at a high signal-to-noise ratio to gain further insights. Finally, the Monte Carlo simulations are performed to verify the correctness of the theoretical results. Numerical results validate the superiority of STAR-RIS-SP-NOMA over STAR-RIS-SP-orthogonal multiple access (OMA) (STAR-RIS-SP-OMA) and the conventional cooperative communication scenarios, such as decode and forward relay-assisted half-duplex-SP-OMA and fixed-gain amplify and forward relay-assisted half-duplex-SP-OMA. We have compared the ABLER expression for all three STAR-RIS operating protocols. Also, the effect of various parameters, such as the ipCSI correlation factor, ipSIC factor, blocklength, information bits, and number of STAR-RIS elements on the system performance is examined.</p>
59.	<p>Performance evaluation of coded cooperation system using software defined radios A Ashok, BW Yu, S Bhattacharyya, S Darshi, JY Pan - IEEE Sensors Journal, 2025</p> <p>Abstract: One of the groundbreaking innovations that is predicted to revolutionize transportation in the future and improve the quality of life is autonomous driving. To ensure on-road safety in such scenarios, the reliable exchange of basic safety messages (BSMs) is important which has been an ever-growing challenge owing to the rising traffic density. The introduction of network-coded cooperation (NCC) in vehicle-to-vehicle (V2V) scenarios has greatly enhanced the performance of vehicular networks in terms of bit error rate (BER) and throughput. Such technologies need to be implemented and validated comprehensively before being deployed in real-life transportation systems to meet the required quality-of-service (QoS). However, due to the inherent complexities of hardware, the practical implementation of NCC has been less explored. In this paper, we thus implement an NCC-based system practically using multiple universal software radio peripheral (USRP) devices to serve as the on-board units (OBUs). Workflows have been proposed based on which the USRPs have been designed. To check the authenticity of the proposed workflows in providing reliability, metrics like BER and throughput are considered for the work. The results obtained are compared with other relevant schemes. Despite the complicated nature and stochasticity of the hardware implementation, the findings obtained via multiple iterations indicate enhanced BER improvements of 10.956% and 2.888%, and throughput gains of 9.6% and 1.32%, over the relayed and direct paths, respectively. These gains in reliability and throughput are vital for vehicular systems. Finally, to acquire additional insights, the results obtained using USRP have been compared with their respective simulation results, which show an impressive correlation with each other by following a similar trend.</p>  <p style="text-align: center;">On- Road scenario Lab Set-up</p>
60.	<p>Phase transformation pathways and mechanical behavior of heat-treated direct metal laser sintered additively manufactured Ti6Al4V alloy BP Mahto, A Tripathi, AG Rao, R Kumar, RK Rai, MK Mishra - Metallurgical and Materials Transactions A, 2025</p>

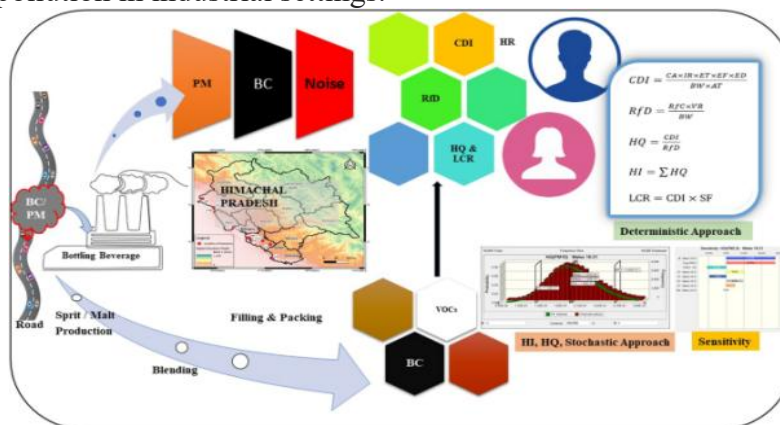
Abstract: The current work focuses on phase transformation pathways and the correlation between microstructure and mechanical properties of heat-treated direct metal laser sintered additively manufactured Ti6Al4V alloy. As-printed sample consists of acicular α' with heterogeneously distributed nano β particles. However, after heat treatment, heterogeneity of the β phase was reduced and morphology of the β phase was modified to rod shape. Mechanical properties are influenced by α/α' lath size and extent of decomposition of acicular $\alpha' \rightarrow \alpha + \beta$. Moreover, high fraction of β phase and presence of both particle and rod shape β counteracts the effect of larger α'/α lath thickness on decreasing ductility. The best combination of tensile strength (1193 ± 5 MPa) and ductility (17.1 ± 0.45 pct) was achieved through the phase transformation pathway; $(\alpha' + \text{non-uniformly distributed nano } \beta \text{ particles}) \rightarrow (\beta + \text{primary } \alpha) \rightarrow (\text{primary } \alpha + \alpha' + \text{few nano } \beta \text{ particles}) \rightarrow (\text{primary } \alpha + \alpha/\alpha' + \text{uniformly distributed nano } \beta \text{ particles})$.

[Potential health risk estimation through deterministic and stochastic approach for the air pollutants found inside bottling beverage industries of Himachal Pradesh in India](#)

I Dhada, P Vats, SK Samal - Discover Environment, 2025

61.

Abstract: The rapid advancement of global industrialization has significantly increased air pollution, particularly particulate matter (PM), black carbon (BC), and noise, impacting indoor air quality in urban areas and posing notable health risks. This study monitored total volatile organic compounds (TVOCs), noise, PM (PM_{10} , $\text{PM}_{2.5}$, PM_1), and BC inside bottling and beverage industries during the monsoon season in Himachal Pradesh, India. The highest recorded values of parameters were 142 ppm (TVOC), $359 \mu\text{g}/\text{m}^3$ (PM_{10}), $102 \mu\text{g}/\text{m}^3$ ($\text{PM}_{2.5}$), $65 \mu\text{g}/\text{m}^3$ (PM_1), $26 \mu\text{g}/\text{m}^3$ (BC), and 87 dB (noise). The health risk assessment revealed noncarcinogenic hazard ratios (HRs) ranging from 0.52 to 0.80, with the highest risk observed for males aged 50–60 and females aged 40–50. Carcinogenic risk attributed to BC was estimated between $5.8\text{E}-04$ and $6.8\text{E}-04$. The highest uncertainty (2.02%) was observed in the carcinogenic risk for BC among females aged 21–30. In comparison, the lowest uncertainty (0.36%) of risk was found in noncarcinogenic HR for $\text{PM}_{2.5}$ among males of the same age group. While minimal variation for HR estimation ($\sim 0.87\%$) was found between deterministic and probabilistic approaches. Despite limitations inherent to its cross-sectional design, the study underscores significant occupational health risks due to indoor air pollution in industrial settings.



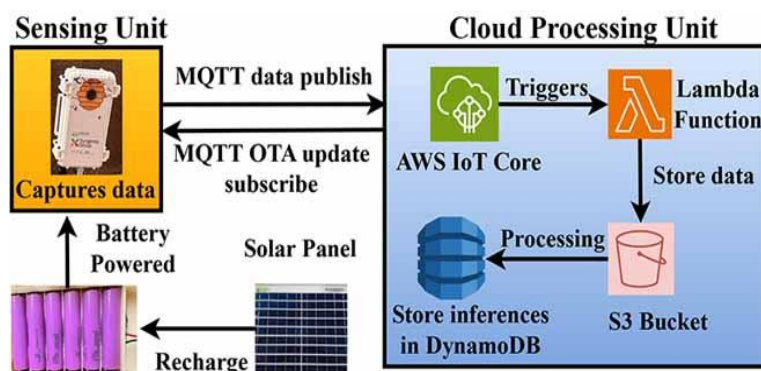
[Power and memory-efficient Low-Cost IoT sensing system for biodiversity surveillance developed on resource-constrained platform](#)

K Singh, M Kaur, S Kumar - IEEE Sensors Journal, 2025

62.

Abstract: Imperative demand is arising for biodiversity surveillance due to the decline in certain insect species. Existing biodiversity surveillance systems depend on high-end processors and heavy operating systems (OSs) that require numerous packages, resulting in increasing complexity and power consumption. In contrast, resource-constrained IoT platforms are low-cost and requires

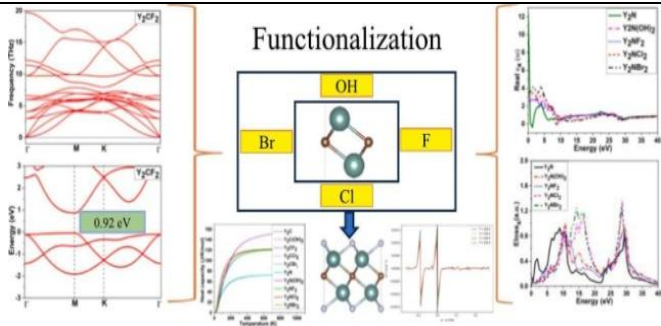
minimal code footprints for operation, resulting in reduced complexity. However, due to the resource scarcity of such platforms, it is required to integrate efficient management strategies for handling a large volume of data generated by the surveillance system. To address this, a low-cost sensing system on a resource-constrained platform is developed that offers power-efficient biodiversity monitoring through a proposed task-scheduling architecture. The system employs the message queuing telemetry transport (MQTT) protocol for the publish-subscribe paradigm. However, the existing JavaScript object notation (JSON) based MQTT payload format limits the payload size for transmission and increases random-access memory (RAM) utilization. To overcome this issue, a raw binary MQTT transmission pipeline is proposed which maximizes the payload size while reducing RAM usage and transmission time, leading to lower energy consumption compared to JSON-based transmission. Furthermore, the proposed over-the-air (OTA) update framework enables remote updates to system configurations. Graphical and tabular comparisons of current consumption, battery lifetime, and cost demonstrate that the designed sensing system outperforms the existing DarkNet53, PICT, and Moth traps systems. Moreover, the presented cloud pipeline architecture provides insect species inferences with an approximate precision of 97%.



[Properties of yttrium based MXenes and the effect of its functionalization: A DFT study](#)
A Pandey, N Sardana - FlatChem, 2025

63.

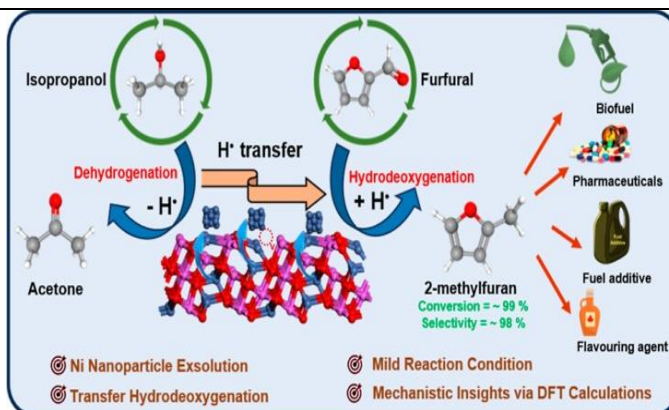
Abstract: This article explores the implications of surface functionalization with hydroxide, fluorine, chlorine, and bromine functional groups on structural, dynamical, mechanical, electronics, optical and thermal characteristics of single layer Y_2XZ_2 MXenes (X signifies C or N, Z corresponds to OH, F, Cl, and Br) with the help of Vienna Ab initio Simulation Package (VASP). The outcomes show that functionalization considerably influences the vibrational, mechanical, electronics, thermal and optical properties of Y_2XZ_2 . Notably, functionalization increases its mechanical properties. Furthermore, functionalization converts metallic characteristics of Y_2C MXenes into semiconductor behavior, but Y_2NZ_2 retain their metallic nature. Real and imaginary components of dielectric function also depend on specific functional groups. In the NIR region, Y_2N showed a negative magnitude of real part. Importantly, a correlation has been observed between the band gap and Seebeck coefficient, higher band gaps resulting in higher values of Seebeck coefficients at a given temperature. These findings have significant implications for the development of advanced technology in nanoelectronics and optoelectronics fields.

	 <p>The figure is a composite of several plots and a central diagram. On the left, two band structure plots for TiO_2 show energy levels (eV) versus momentum. The top plot shows a band gap of 0.92 eV. In the center, a 'Functionalization' diagram shows a central molecule with OH, Br, F, and Cl groups. On the right, two plots show conductance (in units of $2e^2/h$) versus energy (eV) for different systems: TiO_2, $TiO_2(OH)_2$, TiO_2F_2, TiO_2Cl_2, and TiO_2Br_2. The bottom plot shows a conductance histogram with peaks corresponding to different states.</p>
64.	<p>Quantum conductance states in Ni/Mo/MoO₃/Ni memristors: Implications for multi-level neuromorphic computing M Praveen, AK Nishad, VK Nishad - Journal of Physics D: Applied Physics, 2025</p> <p>Abstract: This study examined conductance quantization (CQ) in Ni/Mo/MoO₃/Ni memristors using an electrothermal model in COMSOL Multiphysics. Oxygen ions moving in MoO₃ cause the formation and rupture of conductive filaments, making them very thin and leading to quantum effects on the device conductance. As a result, the memristor showed ten stable states near integer and half-integer multiples of the quantum conductance unit ($G_0 = 2e^2/h$) when a DC voltage was applied at room temperature. An analysis of the CQ states under different compliance currents (ICC) and voltage ramp rates (VRR) showed important behaviors: the number of CQ states increased with ICC until it leveled off, and a higher VRR resulted in a steady drop in the CQ states. These results provide important information for improving the memristor performance under different electrical conditions, aiding their use in neuromorphic computing systems. The CQ states in the Ni/Mo/MoO₃/Ni memristors can potentially reduce the hardware requirements of neuromorphic systems by up to 62.5%. The simulation results also highlight the potential of using quantum conductance states for efficient neuromorphic computing, with the proposed memristor achieving approximately 97.56% accuracy in recognizing MNIST digits using a feedforward neural network (FNN). This study provides a promising direction for the development of advanced, multi-level neuromorphic systems.</p>
65.	<p>Quasi-probability distribution of work in a measurement-based quantum Otto engine C Purkait, S Dasgupta, A Biswas - Physica A: Statistical Mechanics and its Applications, 2025</p> <p>Abstract: We study the work statistics of a measurement-based quantum Otto engine, where quantum non-selective measurements are used to fuel the engine, in a coupled spin working system. The working system exhibits quantum coherence in the energy eigenbasis at the beginning of a unitary work extraction stage in the presence of inter-spin anisotropic interaction. We demonstrate that the quasi-probability of certain values of stochastic work can be negative, rendering itself akin to the quasi-probability distribution found in phase space. This can be attributed to the interference terms facilitated by quantum coherence. Additionally, we establish that coherence can improve the average work in finite time. Subsequently, we compare the work distribution with that of a quantum Otto engine that operates between two heat baths in a conventional setting. We find that, because of the absence of quantum coherence, the quasi-probability of stochastic work cannot be negative in a standard quantum Otto engine.</p>
66.	<p>RF FSO integration for hand-off reduction in CRAN assisted vehicular networks B Kumbhani, SK Singh, R Singh, S Darshi, G Singh, I Sharma, E Leitgeb, B Eichberger, KA Shah - Journal of Optics, 2025</p> <p>Abstract: The ever-increasing throughput demand is aimed to be met by the combined use of the radio frequency (RF) and free space optical (FSO) spectrum. However, making this combination into practice is still uncertain, especially for high-mobility scenarios with a limited coherence window for beam training and tracking. Accordingly, significant research efforts are being made</p>

	<p>towards the integrated RF and FSO framework. In this paper, we propose an integrated framework that makes use of the RF spectrum with the FSO spectrum to serve vehicles that are moving under the coverage of a cloud radio access network (CRAN). The proposed scenario simultaneously exploits the advantages of large distance coverage and a huge spectrum from RF and FSO, respectively. It poses the challenge of higher attenuation of FSO through the coordinated multi-point (CoMP) transmission for users being served by FSO spectrum. At the same time, the proposed framework takes care of the high attenuation of RF signals under poor weather conditions, e.g., rainy conditions, by providing a hybrid link with the FSO spectrum. Furthermore, the simulation results show that a reduction of hand-off is observed through the proposed scheme of integration of RF with FSO spectrum in the CRAN-assisted vehicular networks.</p>
67.	<p>Rheology and electro-magnetism stimulated non-trivial deformation dynamics of viscoelastic compound droplets P Gupta, P Dhar, D Samanta - Proceedings of the Royal Society A: Mathematical, Physical and Engineering Sciences, 2025</p> <p>Abstract: In this research, we present an analytical model describing the deformation dynamics of viscoelastic, leaky dielectric droplets confined within a surrounding liquid under the influence of direct electric field and uniform magnetic field. We have considered various combinations of droplets and surrounding fluid, which can be either Newtonian (N) or non-Newtonian (N-N), and may mimic a compound droplet scenario too. The governing equations for conservation of charge, mass, momentum and electromagnetic phenomena are solved for the leaky dielectric theory within the Stokes flow regime and the small deformation approximation. The electrical, magnetic and viscoelastic behaviour is realized using the Cauchy momentum equation in conjunction with the Maxwell stress tensor, Lorentz force and the upper convected Maxwell model, respectively. The changes in deformation and flow characteristics are comprehensively analysed through the variation of key non-dimensional parameters, namely the Capillary number (Ca), Weissenberg number (Wi) and electromagnetic interaction number (Em). The present work is restricted to $Wi \leq 1$ and semi-analytical solutions to the complicated multi-physics phenomena are obtained. Our study reveals that in the presence of only an electric field, a flow field in the non-Newtonian fluid fails to develop if the droplet has relatively lower conductivity compared with the surrounding medium, owing to the insufficient intensity of the electric field. However, when the droplet is relatively more conductive than the surrounding medium, a flow field does arise. The analysis shows that an augmentation in the flow and deformation behaviour of the non-Newtonian fluid can be observed when the magnetic field is applied, but only in a specific direction relative to the electric field. Flow is induced in the $+B$ direction when the droplet is relatively less conductive, and the electromagnetic force dominates over the hydrodynamic force. Conversely, in the $-B$ direction, flow is induced when the droplet is relatively more conductive, as both the electric and electromagnetic forces act together. Such findings provide intricate insights into understanding electro-magneto-hydrodynamics with non-Newtonian confined droplets, and may enable avenues towards realizing precision industrial and scientific microfluidic technologies via manipulation of the movement, deformation and coalescence of droplets.</p>
68.	<p>Singular twisted links and singular twisted virtual braids N Komal, M Prabhakar - International Journal of Mathematics, 2025</p> <p>Abstract: The concepts of the twisted knot theory and the virtual singular knot theory inspire the introduction of the singular twisted knot theory. This research presents comparable results for singular twisted links, such as the Alexander and Markov theorems derived from virtual knot theory. However, it differentiates itself from virtual singular knot theory by demonstrating that the number of Markov moves can be minimized within this framework. Furthermore, this paper introduces singular twisted virtual braids and explores their monoid structure. We also offer a monoid presentation and a reduced monoid presentation for singular twisted virtual braids.</p>

69.	<p>Spatial distribution analysis of soil radioactivity using gamma-ray spectroscopy and radiological inferences M Prasad, P Semwal, SS Kaintura, V Ayri, K Singh, M Joshi, SC Uniyal, PP Singh, RC Ramola - The European Physical Journal Special Topics, 2025</p> <p>Abstract: Naturally occurring radionuclides in soil, rocks, and vegetables can be identified and quantified using gamma-ray spectroscopy, one of the most extensively employed techniques. This investigation has been planned and carried out to assess the natural radioactivity due to ^{226}Ra, ^{232}Th, and ^{40}K in soil samples ($N=46$) from Kumaun Himalaya, India using NaI:TI gamma-ray spectrometry. The average values of activity concentrations of ^{226}Ra, ^{232}Th, and ^{40}K were found to be 48 Bq kg^{-1}, 42 Bq kg^{-1}, and 2009 Bq kg^{-1}, with standard deviations of 11 Bq kg^{-1}, 11 Bq kg^{-1}, and 156 Bq kg^{-1}, respectively. With an average value of 264 Bq kg^{-1} and a standard deviation of 30 Bq kg^{-1}, the radium equivalent activity (Ra_{eq}) was significantly below the safe limit of 370 Bq kg^{-1}. However, a few samples were observed to have Ra_{eq} values exceeding the safe limit. The spatial distributions and the inter-correlations of the measured and estimated radiological quantities are presented in the paper. The contributions of ^{226}Ra and ^{232}Th to radiation dose quantities were observed to be approximately equal, whereas that of ^{40}K was observed to contribute most in this study. The anticipated doses from radionuclides were found to be up to three times higher than the global average values. The outcomes of this study offer noteworthy baseline data for future studies. More detailed monitoring and mitigation measures are recommended to minimize the risk of gamma-ray exposure.</p>
70.	<p>Specialized fractionation combined with deep analytics of waste plastic cracking oils for petrochemical operations R Tomar, A Singh, A Karaba, J Moško, KA Gawłowski, N Kumar, M Staf, VS Sikarwar, Michael Pohořelý - Journal of Industrial and Engineering Chemistry, 2025</p> <p>Abstract: Waste plastic cracking oils (WPCO) are currently being considered as potential green feedstock for petrochemical/refinery industries in order to promote chemical recycling. However, the WPCO is a very complex material that does not meet the limits of petrochemical processes. In order to assess the possibility of using WPCO as raw material, a comprehensive analytical characterization and distillation of two wide-boiling WPCO samples from the industry was performed. Fractions boiling in typical ranges were prepared: naphtha ($30\text{--}180^\circ\text{C}$), heavy naphtha ($30\text{--}250^\circ\text{C}$), middle distillate ($180\text{--}350^\circ\text{C}$), and atmospheric residue ($> 350^\circ\text{C}$). Moreover, other distillation cuts were prepared by distilling every 10 wt% as a separate fraction. We performed a study on the distribution of parameters in narrow fractions. The content of aromatics increased with the boiling temperature in the cases of WPCO-1, but decreased for WPCO-2. WPCO-2 had lower alkanes and final boiling point (FBP) compared to WPCO-1. None of the distillation cuts are suitable for “stand-alone” processing on the steam-cracker without additional treatment. However, some of the obtained fractions could be co-processed with a standard feedstock. This study brings an understanding of WPCO material and the possibilities and limitations of its use as petrochemical input.</p>

71.	<p>Sustainable modular biofiltration system with rainshower technology for AQI reform V Jaiswal, S Singh, A Mangal, PP Singh - Scientific Reports, 2025</p> <p>Abstract: India is the tenth most polluted nation in the world, according to the World Health Organization (WHO) 2022 assessment. Approximately 1.67 million deaths are caused by lung, cardiovascular, stroke, and chronic pulmonary obstruction worldwide (WHO 2024). In 2019, 1.36% of GDP was reported to be lost because of air pollution and related issues. The results presented in this article demonstrate the efficacy of UBREATHE RAIN. Ambient (outside), untested enclosure (reception), and tested enclosure (breathing lounge with 3 Ubreathe Rain) were the 3 test venues that were found based on proximity and interaction to the stubble burning site. The Air Quality Index (AQI) was recorded as the highest sub-index of pollutants involved (CO, PM, SO₂, NO₂, and O₃) through grab sampling. Throughout the studies, the AQI in the tested enclosure was ~35% lower than that in the ambient environment and ~30% lower in the untested enclosure. Statistical analysis also supported this finding, as the p-value remains < 5% throughout (p-value ≈ 2%). Additionally, temperature and relative humidity changes were examined and demonstrated to represent significantly less of a challenge to the effectiveness of the proposed technology. The experiment's duration and demographics may have limited the given results and their importance.</p>
72.	<p>Synergistic effect of Ni exsolution and oxygen vacancies in NiAl₂O₄ for catalytic transfer hydrodeoxygenation of furfural to 2-Methylfuran A Kumar, DR Kanchan, A Banerjee, BP Singh, R Srivastava - ACS Catalysis, 2025</p> <p>Abstract: The exsolution of metal nanoparticles from solid lattices provides a strategy for designing efficient catalysts in catalytic transfer hydrodeoxygenation (CTHDO). This approach allows precise control over key catalytic properties, including nanoparticle density, surface acidity, and oxygen vacancies, which are crucial for the optimization of CTHDO reactions. We report a NiAl₂O₄-550 catalyst for the selective CTHDO of furfural (FUR) to 2-methylfuran (2-MF) with high selectivity. Using isopropyl alcohol (IPA) as a hydrogen donor, NiAl₂O₄-550 exhibited a high performance under favorable reaction conditions. Characterization (PXRD, Raman, TEM, XPS, NH₃-TPD, Pyridine-FTIR, and H₂-TPR/TPD) highlights the role of surface oxygen vacancies and exsolved Ni-metal in enhancing catalytic activity. XPS, O₂-TPD, and EPR confirm their contributions to FUR conversion. DFT calculations reveal that oxygen-deficient sites improve substrate–catalyst interactions, lowering the energy barrier for FUR to 2-MF conversion. Under mild conditions (180 °C, 2 MPa of N₂), NiAl₂O₄-550 afforded ~99% FUR conversion with a 98.1% 2-MF selectivity, surpassing that of reported catalysts. The combination of oxygen vacancies and metal exsolution enables controlled transfer hydrodeoxygenation, offering an effective strategy for biofuel production. This study establishes a versatile platform for next-generation catalysts in environmentally conscious catalysis, contributing to advancements in catalyst design.</p>

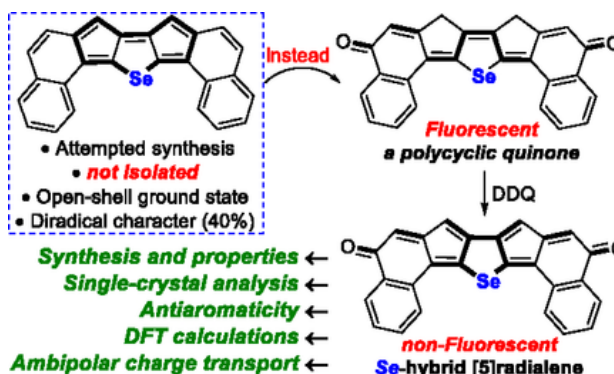


Synthesis of a Seleno-hybrid [5] radialene derivative and exploration of polycyclic heteroterphenoquinones as ambipolar charge carriers

S Sahewal, A Sharma, PK Sharma, D Mallick, UK Pandey, S Das - European Journal of Organic Chemistry, 2025

73.

Abstract: para-Terphenoquinone (pTPQ) in which a benzenoid ring has been replaced with a heterocycle is known as heteroterphenoquinone (HTPQ). While (H)TPQs are typically non-emissive and potentially open-shell species, we recently reported that fully fused polycyclic HTPQs (or PHTPQs) bearing a sulfur heteroatom could either exhibit fluorescence or antiaromaticity depending on the π -conjugation arrangement in the core. Since the synthesis of PHTPQs is rare, until now limited to our own reported compound containing a sulfur atom, we have now synthesized a selenium-containing fluorescent PHTPQ while attempting the isolation of elusive dinaphtho-dicyclopenta[b,d]selenophene. The fluorescent PHTPQ was further dehydrogenated to synthesize the first PHTPQ with an embedded selenophenoradialene (seleno-hybrid [5]radialene), which was found to exhibit antiaromatic properties. The narrow optical HOMO-LUMO gap, short intermolecular interactions in the solid state, and redox amphoterism prompted us to explore its ambipolar charge transport properties alongside the thia-analogue. The electron mobilities for PHTPQs comprising selenaradialene ($1.96 \times 10^{-3} \text{ cm}^2 \text{ V}^{-1} \text{ s}^{-1}$) and thiaradialene ($1.58 \times 10^{-3} \text{ cm}^2 \text{ V}^{-1} \text{ s}^{-1}$) cores were found to be one order of magnitude higher than that of the holes due to low-lying LUMO energy levels.



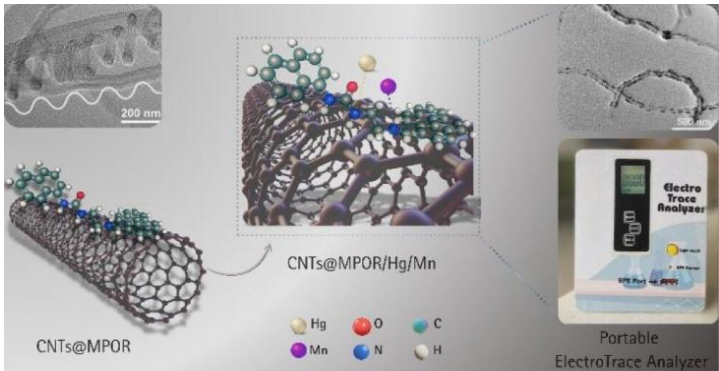
Temperature-driven thermoelectric transition in orthorhombic-ZrS₂ monolayer via first-principles analysis

RP Jadav, J Jasani, Y Sonvane, D Singh, R Ahuja - International Journal of Modern Physics B, 2025

74.

Abstract: Two-dimensional (2D) materials hold immense promise for a wide range of applications due to their exceptional and tunable properties. Among these, transition metal compounds stand

	<p>out for their compositional versatility, enabling precise control of their physical and chemical characteristics. In this study, we systematically investigate the structural, electronic and optoelectronic properties of orthorhombic ZrS₂ (o-ZrS₂), with a focus on the influence of atomic positioning within its lattice. Phonon dispersion analysis confirms the dynamic stability of the structure, while mechanical stability is established through energy–strain relationships derived from elastic constants. Electronic band structure and density of states (DOS) analyses identify o-ZrS₂ as a semiconductor with band gaps of 0.715eV and 1.847eV calculated using PBE and HSE06 methods, respectively, primarily attributed to the overlap of Zr–d and S–p orbitals. Optical absorption spectra demonstrate strong UV light absorption, peaking at 11.8eV with an absorption coefficient of $6.33 \times 10^5 \text{ cm}^{-1}$. Furthermore, thermoelectric analysis reveals a high electronic figure of merit (ZT_e) ranging from 1.022 to 1.073 and high-power factor (PF) of $1.07 \times 10^{11} - 2.503 \times 10^{11}$ over the temperature range of 300–900K. These results underscore the potential of o-ZrS₂ as a high-bandgap semiconductor with excellent UV absorption and thermoelectric performance ($ZT_e > 1$), making it a promising candidate for next-generation thermoelectric devices.</p>
75.	<p>The interplay of SDGs and climate action: A quantitative analysis of regional income influences on SDG 13 progress M Chaurasiya, S Kumar, K Bhatt, S Sharma - Physics and Chemistry of the Earth, Parts A/B/C, 2025</p> <p>Abstract: This research provides a comprehensive examination of the interconnected nature of the Sustainable Development Goals (SDGs) and their combined impact on SDG 13 - Climate Action, focusing on the varying economic contexts of countries worldwide. Utilizing data from 160 countries, the study employs the Extra Trees Regressor and Shapley Additive Explanation (SHAP) values to understand the independent effects of each SDG on climate action under diverse economic conditions. The findings reveal that the progress made in achieving SDGs contributes differently to climate mitigation efforts across various economic classifications. For instance, in high-income countries, the contribution of SDGs related to environmental sustainability is significantly higher compared to low-income countries, largely due to advancements in green practices, urban development, and sustainable production and consumption patterns. The research underscores the critical need to integrate climate action into national plans tailored to a country's specific ecological and economic circumstances. Therefore, region-specific strategies may be necessary for the successful implementation of SDGs and the effective achievement of climate action goals. The study advocates for a dynamic approach to policymaking that acknowledges and leverages SDG interlinkages, fostering global cooperation to achieve comprehensive and equitable sustainability outcomes. This research aims to advance the science of sustainability by elucidating how economic contexts shape the attainment of SDG 13 and provides practical guidance to policymakers for improved global climate action.</p>
76.	<p>Thermal and hydrodynamic behavior in the transitional mixed convection regime for buoyancy-aiding and opposing flows S Gorai, SK Das, D Samanta - Heat Transfer, 2025</p> <p>Abstract: In practical heat exchangers, where tube lengths are typically shorter, the flow is largely developed. In this numerical investigation, we examined the thermal and hydrodynamic characteristics within the transitional developing regime of mixed convection for buoyancy-aiding and opposing flows through a vertical tube. Employing a two-dimensional axially symmetric approach with a steady state, simulations were conducted for a range of Reynolds number ($2000 \leq Re \leq 5000$), Grashof number ($4 \times 10^5 \leq Gr \leq 2.5 \times 10^6$), and Richardson number (Ri) of 0.1 for a nondimensional length (L/D) of 150 subjected to uniform wall heat flux condition. The study involved a comparative analysis of two transition models: transition $\kappa-\kappa_1-\omega$ and transition shear stress transport (SST) and the model with better accuracy was selected. The findings reveal the crucial role of buoyancy in the laminar-turbulent transition for both assisting and opposing flows.</p>

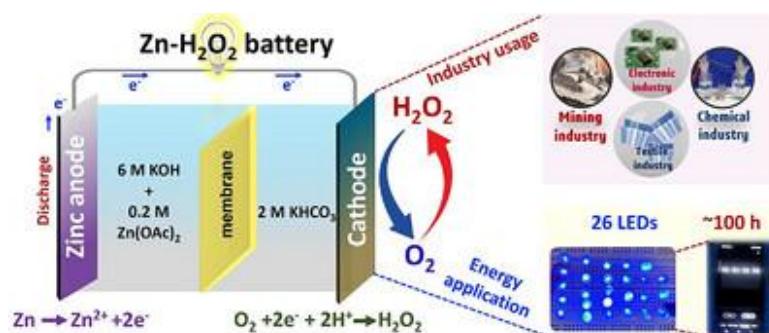
	<p>In both flow scenarios, the coefficient of skin friction (C_f) and Nusselt number (Nu) exhibit an increase with increasing Re at a constant Ri. Notably, under the same Ri conditions, the opposing flow exhibits higher pressure drop (assessed by C_f) and heat transfer (assessed by Nu). For buoyancy-aiding and opposing flows, the hydrodynamic entry length reduces from $L/D \sim 70$ to 60, while the thermal entry length extends with increasing Gr and Re, when Ri is fixed. Furthermore, the onset of transition in mixed convection is dependent on the wall heat flux and is earlier in opposed flow than assisted flow. Based on the intermittent behavior, the lower transitional zone ($2000 < Re < 3000$) and the higher transition zone ($3000 < Re < 5000$) have been demonstrated.</p>
77.	<p><u>Transient analysis of electromagnetic waves on DNG metamaterial slab backed by PEC</u> S Bhattacharjee, B Kumbhani, SK Singh - Physics Letters A, 2025</p> <p>Abstract: This paper is based on time domain analysis of electromagnetic field incident normally on double negative (DNG) metamaterial slab backed by perfect electric conductor (PEC). Electromagnetic fields are analyzed based on double exponential pulse being incident over PEC backed DNG metamaterial slab. Further, the strength of reflected fields from the interface between air and DNG slab, and transmitted fields in DNG slab are evaluated analytically. Evaluated results in terms of amplitude of reflected pulse and transmitted pulse are plotted both for Double Positive (DPS), i.e. dielectric and DNG metamaterial cases. Thus, the effect of both PEC backed DPS & DNG metamaterial slab are investigated and compared.</p>
78.	<p><u>Ultrasonically driven structural evolution of bimetallic heterostructures for construction of an electrotrace analyzer</u> R Kaur, Sonam, G Bhardwaj, N Goel, N Singh, N Kaur - Langmuir, 2025</p> <p>Abstract: Bimetallic heterostructure materials (BHMs) have garnered significant attention due to their exceptional synergistic electrocatalytic properties. However, challenges persist in developing precise, scalable synthetic methods and understanding their underlying mechanisms. Here, we develop an ultrasonic-assisted anchoring strategy to fabricate BHMs on multiwalled carbon nanotubes (MWCNTs). First, a multifunctional polyaromatic organic receptor (MPOR), featuring urea and imine functional groups, was physisorbed onto MWCNTs (MWCNTs@MPOR), inducing structural coiling. Subsequent interaction with Hg metal ions led to the reorganization of MWCNTs (MWCNTs@MPOR/Hg), followed by ultrasonic treatment that facilitated Mn ion anchoring at the free imine sites, yielding the final BHMs MWCNTs@MPOR/Hg/Mn. Notably, the structural changes and nature of interactions were thoroughly studied by density functional theory (DFT) simulations. Experimental results and first-principles calculations revealed remarkably enhanced electrochemical activity with a charge transfer of $-0.179e$ in MWCNTs@MPOR/Hg/Mn. Further, we introduced a portable “ElectroTrace Analyzer” based on MWCNTs@MPOR/Hg/Mn for real-time detection and quantification of atrazine (herbicide). Our ultrasonically assisted strategy for BHM synthesis offers a fascinating avenue for the advanced development of useful BHMs for real-world applications.</p>  <p>The figure illustrates the synthesis and application of bimetallic heterostructures. It includes a schematic of the synthesis process, a 3D model of the structure, and a photograph of the portable device. The schematic shows the synthesis of MWCNTs@MPOR, followed by the addition of Hg and Mn to form MWCNTs@MPOR/Hg/Mn. The 3D model shows the structure of MWCNTs@MPOR/Hg/Mn. The photograph shows the portable ElectroTrace Analyzer device.</p>

79.	<p>Understanding the impact of Aravalli hills mining on groundwater contamination of Delhi, India A Gani, S Pathak - Environmental Geochemistry and Health, 2025</p> <p>Abstract: Groundwater contamination poses a significant threat to public health and environmental sustainability, particularly in regions impacted by anthropogenic activities such as mining. The purpose of this study was examining the degree of groundwater contamination in Delhi, India, particularly regarding the effects of mining operations in the Aravalli Hills. This study uses an integrated approach that includes the water quality index (WQI), modified heavy metal pollution index, human health risk assessment (HHRA), and geospatial techniques to evaluate the effects of mining on groundwater quality. Data of various physiochemical parameters and heavy metals were collected from the Central Groundwater Board for the year 2023–24. The WQI was calculated by using a hybrid aggregation technique and human health risk was assessed due to the ingestion and dermal contact by using the United States Environmental Protection Agency model. The WQI of the Delhi varies from 2.15 to 94.03. Results of WQI concluded that the groundwater quality of Delhi state was mostly lie in the category of poor to very poor quality, indicating serious deterioration. According to the results of HHRA, the value of total hazard index (THI) was varying from 0.86 to 49.25 for infants, 0.39 to 33.62 for children, 0.18 to 15.71 for teens and 0.16 to 13.72 for adults. The spatial distribution of WQI, THI and cancer risk were further mapped using geospatial mapping techniques, which also connected them to certain mining zones and geological vulnerabilities. In order to reduce contamination and safeguard public health, finding of the study highlights the urgent need for groundwater management plans, sustainable mining methods, and regulatory actions. In order to encourage water conservation measures and lower the release of pollutants into the environment, public awareness campaigns and community involvement should also be crucial. SDG 6 goals may be further supported by funding groundwater recharge projects and cutting-edge treatment technology, which will restore damaged aquifers and guarantee that everyone has access to safe water.</p>
80.	<p>Unlocking long life aqueous zinc-sulfur rechargeable battery derived from zinc waste powering 30 LEDs S Mehta, M Singh, K Garg, RN Mishra, K Kumar, M Moirangthem, SK Meena, TC Nagaiah - Advanced Energy Materials, 2025</p> <p>Abstract: Aqueous Zinc-sulfur (Zn-S) rechargeable batteries are emerging as promising next-generation energy storage devices due to safety, capacity, cost and efficiency. However, Zn corrosion, polarization, low conductivity and volume expansion of sulfur cathode are the bottlenecks for battery stability and capacity. Herein, we report a dual strategy involving sulfanilamide (SA) as additive to stabilize Zn, paired with hollow $\text{Ni}_x\text{Fe}_y\text{O}_4$ to confine sulfur, mitigating volume expansion and enhancing conductivity along with iodine as redox mediator to improve the Zn^{2+} kinetics. The designed battery demonstrated an excellent specific capacity of 1260 mAh g^{-1} at 0.1 C with 81% capacity retention after 1000 cycles at 1 C. The SA mitigates the hydrogen evolution reaction (HER) by 3.5 times and 2.8-fold reduction in corrosion rate of Zn anode, which is, supported by Raman, and ^1H NMR spectroscopy and further complimented by computational studies. The symmetric $\text{Zn} \text{Zn}$ cell with SA was stable for more than 770 h, demonstrating an ultra-high stability of Zn anode. Formation of ZnS was monitored by electrochemical in-situ Raman spectroscopy. The designed Zn-S homemade pouch cell powered a panel of 30 red LED for 93 h and furthered powered fan, demonstrating exceptional sustainability.</p>

[Unveiling an In-situ H₂O₂ production: Rechargeable Zinc-H₂O₂ battery powering 26 LEDs](#)
S Mehta, S Kaur, K Garg, M Singh, T C. Nagaiah - Angewandte Chemie, 2025

81.

Abstract: Looking toward ever-growing energy demand, the advancement in energy storage devices and carrying out electrocatalytic reactions in an efficient way is the need of the hour. Herein, we have employed the two birds-one stone approach, viz. fusing energy conversion and storing system enabling $2e^-$ oxygen reduction reaction (ORR) to value-added hydrogen peroxide (H₂O₂) product and its utilization in the energy storage devices using MnWO₄ catalyst, without any external H₂O₂ source. The designed catalyst exhibited a remarkable H₂O₂ production of 98% @ 0.37 V versus RHE. The real-time H₂O₂ production was monitored by in-situ electrochemical Raman and in-situ infrared spectroscopic measurements. The pivotal influence of electrolyte composition, viz. local pH and the formation of carbonate species on H₂O₂ production was meticulously examined through micro-electrochemical studies using gold (Au) microelectrodes. Further, we have explored an aqueous rechargeable Zn-H₂O₂ battery utilizing MnWO₄ as bifunctional electrocatalyst for sustainable H₂O₂ production simultaneously producing the electricity. The Zn-H₂O₂ battery exhibited a remarkable cycle life of 136 h and an practical energy efficiency of 43%. The galvanostatic charge–discharge measurement of Zn-H₂O₂ battery attained a capacity of 25 mAh cm⁻² at 3 mA cm⁻². The battery also demonstrated ≥90% cycle efficiency. Interestingly, the designed Zn-H₂O₂ battery (two connected in series) exhibited a stable open circuit voltage (OCV) with a promising power density of 10.5 mW cm⁻². As a proof of concept, we have demonstrated Zn-H₂O₂ batteries by powering 26 blue LEDs for more than 180 h (7 days) without fading in the illumination of LEDs.



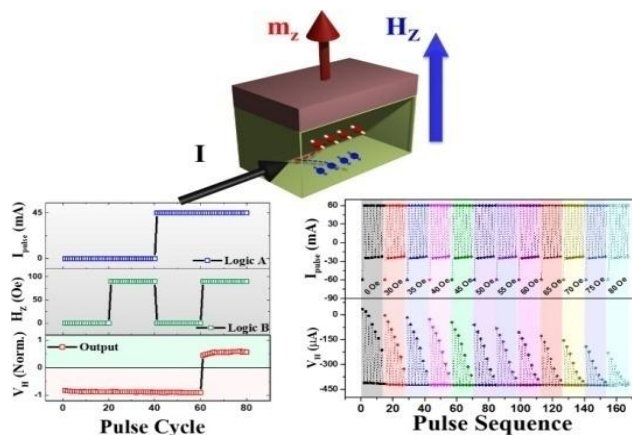
[Versatility of spin-logic and high-density multistate memory enabled by a single spin–orbit torque device](#)

R Posti, A Ravindran K, D Tiwari, D Roy - ACS Applied Electronic Materials, 2025

82.

Abstract: Non-volatile devices based on the spin–orbit torque (SOT) mechanism are suitable for in-memory logic operations. The current objective is to enhance the memory density of memory cells while performing logic operations within the same memory unit. The present study demonstrates that integrating SOT with an out-of-plane magnetic field effectively achieves multiple magnetic states in perpendicularly magnetized heterostructures. This study further explores this approach, experimentally demonstrating versatile logic operations within a single SOT device using W/Pt/Co/AlO_x heterostructures. Our results show that multistate tuning by SOT integration with an out-of-plane magnetic field enables versatility in logic operations, including AND, OR, NOR, NAND, and Always ON, within a single device. Additionally, we found that the careful selection of input logic operations allows multiple configurations to achieve the same logic function within a single memory device. To enhance the multistate memory density, we proposed and experimentally verified a two-step writing process, achieving the highest reported multistate memory density in SOT-based memory devices. These findings highlight the potential of

integrating SOT and magnetic field effects to realize high-density, multifunctional, in-memory logic devices.



Disclaimer: This publication digest may not contain all the papers published. Library has compiled the publication data as per the alerts received from Scopus and Google Scholar for the affiliation “Indian Institute of Technology Ropar” for the month of May, 2025. The author(s) are requested to share their missing paper(s) details if any, for the inclusion in the next publication digest.